Haptic-enabled Robotic Arms to Achieve Handshakes in the Metaverse

by

Mohd Faisal

A thesis submitted to the University of Ottawa
in partial fulfillment of the requirements for the
MASc degree in Electrical and Computer Engineering

Ottawa-Carleton Institute for Electrical and Computer Engineering
School of Electrical Engineering and Computer Science
Faculty of Engineering
University of Ottawa

Abstract

Humans are social by nature, and the physical distancing due to COVID has converted many of our daily interactions into virtual ones. Among the negative consequences of this, we find the lack of an element that is essential to humans' well-being, which is the physical touch. With more interactions shifting towards the digital world of the metaverse, we want to provide individuals with the means to include the physical touch in their interactions. We explore the Digital Twin technology's prospect to support in reducing the impact of this on humans. We provide a definition of the concept of Robo Twin and explain its role in mediating human interactions. Besides, we survey research works related to Digital Twin's physical representation with a focus on under-actuated Digital Twin's robotic arms. In this thesis, we first provide findings from the literature, to support researchers' decisions in the adoption and use of designs and implementations of Digital Twin's robotic arms, and to inform future research on current challenges and gaps in existing research works.

Subsequently, we design and implement two right-handed under-actuated Digital Twin's robotic arms to mediate the physical interaction between two individuals by allowing them to perform a handshake while they are physically distanced. This experiment served as a proof of concept for our proposed idea of Robo Twin. The findings are very promising as our evaluation shows that the participants are highly interested in using our system to make a handshake with their loved ones when they are physically separated. With this Robo Twin Arm system, we also find a correlation between the handshake characteristics and gender and/or personality traits of the participants from the quantitative handshake data collected during the experiment. Moreover, it is a step towards the design and development of Digital Twin's under-actuated robotic arms and ways to enhance the overall user experience with such a system.

Acknowledgments

I would like to express my sincere gratitude to my supervisor, Professor Abdulmotaleb El Saddik, and co-supervisor, Professor Emil Petriu for all their enlightening advice, support, careful guidance, and above all tremendous patience for my entire graduation period at the University of Ottawa. The broad scientific vision and rigorous attitude of my supervisor have deeply affected me both academically and personally. I am very proud of being one of his students.

I would also like to sincerely thank my mentor Professor Fedwa Laamarti, for providing me with constructive feedback and keeping me motivated throughout. This work would have never been possible without her valuable guidance and support.

Special thanks to my colleagues Roberto Alejandro Martinez and Rahatara Ferdousi from the Multimedia Communications Research Laboratory at University of Ottawa for giving me a friendly environment at the Lab, and my friend Abhijeet Singh, an MASc student in Information Technology at the Carleton University for his valuable insights and help with the assembly. A special mention to Justine, manager of Makerspace lab for providing access to the lab and help in 3D printing the robotic hand parts as and when needed.

Finally, I am very grateful to my family and friends especially my mother and sister for all their love, patience and emotional support that was imperative to survive this journey and to help me become the person I am today.

Table of Content

List of Abbreviations

MW	Mirror Worlds
CAD	Computer Assisted Model
DT	Digital Twin
RT	Real Twin
AI	Artificial Intelligence
ASIMO	Advanced Step in Innovative Mobility
FDM	Fused Deposition Modelling
FFF	Fused Filament Fabrication
PLA	Poly Lactic Acid
ABS	Acrylonitrile Butadiene Styrene
PET-G	Polyethylene terephthalate Glycol
PA-12	Nylon
HIPS	High Impact Polystyrene
ASA	Acrylonitrile Styrene Acrylate
TP-UA	Tendon Pin Under-Actuated
IMU	Inertial Measurement Unit
DOF	Degree of Freedom
PEDOT: PSS	Poly (3,4-Ethylene Dioxy Thio-phene) Polystyrene Sulfonate
PDMS	Polydimethylsiloxane
NTC	Negative Temperature Coefficient
PVC	Poly Vinyl Chloride
TLC	Thermochromic Liquid Crystal
HSV	Hue Saturation Value
FSR	Force Sensitive Resistor
ADC	Analog to Digital Converter
USART	Universal Synchronous Asynchronous Receiver Transmitter
ERM	Eccentric Rotating Mass

List of Figures

List of Tables

1. Introduction

1.1 Background and Motivation

The development of the digital immersive technology is accelerated with the introduction of 'Metaverse', the future of the internet. This technology is expected to fade the difference between the physical and the virtual worlds by providing a fully immersive experience to the users of the internet [1], [2]. With more daily interactions shifting towards the digital world of metaverse, providing physical touch in these interactions can enhance the overall user experience. Humans are social beings and physical touch plays an important role in our mental well-being. Conversely, many interactions that used to routinely happen in the real world, have now converted to the virtual world instead because of physical distancing which was widely adopted worldwide to content the spread of new coronavirus SARS-CoV-2 causing the disease COVID-19. However, the research on interaction between virtual world and real world started a few years back and may provide some answers to this issue.

David Gelernter introduced the concept of Mirror Worlds (MW) as a "software models of some chunk of reality" [3]. In Gelernter original idea, one had to create a Computer Assisted Model (CAD) of the real world and that model would receive vast amounts of information from the real object to a point where the "mirror world" would be able to reproduce real world in detail. The mirror worlds were intended to help people better understand and explore reality through a virtual interface. One could have a mirror world of a university with models of students, buildings, bank accounts, faculties and every real-world object could have a counterpart in the "mirror world". The idea was then picked-up by Michael Grieves, who took it further by introducing the concept of Digital Twin (DT) [4]. A DT is actionable, which means that the model can simulate the effects of external forces applied to elements in the model itself.

Alam et. al [5] took Grieves definition of DT to extend it and introduce a DT architecture reference model that augments the original DT idea by establishing the existing relations between the different Real Twins (RTs) and pushing their data to the cloud. This means that the DT is not only a copy of a RT and its internal processes but also holds a copy of its interactions

with other RTs. However, El Saddik raises the question: How can a DT interact directly with the real world on behalf of its RT? The answer that El Saddik suggests combines Artificial Intelligence (AI), sensors, and actuators [6]. This will be useful in situations where the DT is required to act in the real world on behalf of the RT. El Saddik also emphasizes on the need of high-speed networks to ensure 'Quality of Experience (QoE) powered Communications' for the interaction between DT and its RT [7]. A modular framework in [8] provides an automatic recognition and configuration of DT of a physical device and reflects its characteristics and sensory data to be used in either real time or post routine analysis.

A DT can interact with the real world directly by rendering a representation of the RT. The range of options to represent a RT include but are not limited to a robot, hologram, an avatar or simply a software entity sending messages to other systems. A robot can use haptics, speech, or sound, and more. However, a software entity could be limited to using network messages. The DT as suggested by El Saddik can model relations and interact directly with the real world. El Saddik et. al introduced a system to design DTs that lay-out the necessary tools and technologies to implement a DT for health and well-being [9], [10]. In recent years, there has been a visible surge in the number of publications on DT for health and well-being [11] indicating more and more researchers are utilising the DT technology platform to suggest better health services and improving the overall well being of the individuals.

We propose the concept of Robo Twin, which is conceived as a mediator of physical interaction. It aims at providing a form of haptic interaction between individuals, which feels as close as possible to an actual physical contact with others. We believe that to achieve such an immersive experience, we need to provide the Robo Twin with a "body" that feels as close as possible to the body of a human and the capacity to capture touch-related information. In other words, the Robo Twin should be able to convey the sense of touch as accurately as possible, such as in a situation of handshake interaction for example.

Handshaking is also more than a greeting gesture; it conveys a lot more about the person. Indeed, existing research has shown that based on one's handshaking characteristics we can comment on this person's gender and personality traits [12]–[14]. Although most of these research studies

have their own shortcomings, with our Robo Twin system we intend to overcome some of them by including sensor-based measurement of participants handshaking characteristics and using a more precise and independent way of assessing participants personality traits.

As a first step towards this concept, we survey the research works related to the design and implementation of anthropomorphic robot hands to support our decision in the use and improvement of existing designs and implementations of a DT's robotic physical representation, with a focus on the robotic arm. Based on our gathered information, we have been motivated to design and implement the under-actuated DT's robotic arms to imitate the human handshake as closely as possible, while the subjects being physically separated by a distance.

1.2 Thesis Objective & Contributions

The objective of this research is to develop the physical representation of the Digital Twin with focus on the robotic arm to mimic the human handshake as accurately as possible allowing distant individuals to shake hand with one another. This can be achieved in several contributions as mentioned below:

1. Design and implementation of two robotic arms for DT with close to human handshake like ability.
2. Analysis and development of an experiment to determine, accurate placement of temperature and pressure sensors on both Robo Twin arms for sensible collection of human handshake data.
3. Design and development of a handshake system with sensing and actuation capabilities, allowing the bidirectional transmission of haptic data across two Robo Twin arms.

1.3 Thesis Organization

The remainder of this thesis is organized as follows:

- ✓ In Chapter 2, we review the background literature related to the work presented in this thesis.

- ✓ In Chapter 3, we discuss the proposed concept of Robo Twin and its system architecture consisting of sensing, processing, data collection and data transmitting and receiving modules in detail.
- ✓ In Chapter 4, we discuss the overall implementation of Digital Twin's robotic arm to perform the handshake. This chapter details the Robo Twin's arm implementation, its sensors and actuator's selection, calibration, placement, and implementation.
- ✓ In Chapter 5, we present both the quantitative and qualitative evaluation of the proposed Robo Twin system designed for the purpose of human handshake.
- ✓ Finally, in Chapter 6, we present our conclusions, and provide potential future work.

1.4 Scholastic Output

The following publications have been contributed through this research work.

1. **Mohd Faisal**, Roberto Alejandro Martinez Velazquez, Fedwa Laamarti and Abdulmotaleb El Saddik. "Under-Actuated Digital Twin's Robotic Hands with Tactile Sensing Capabilities for Well-being." Digital Twin for Healthcare: Design, Challenges and Solutions, Elsevier, 2022.

2. Related Work

In this chapter, we review the existing literature in the field of Digital Twin robotic representation with a focus on under-actuated Digital Twin robotic arm. With this background research we aim at providing findings from the literature, to support researchers' decision in the adoption and use of existing designs ad implementation of Digital Twin's robotic hands, and to inform the future research on current challenges and gaps in the existing research work.

2.1 Humanoid robots

Humanoid robots are complex anthropomorphic artificial machines. The growing interest in humanoid robots accompanied by the latest and ever-increasing technological advancements in the field of robotics, locomotion, and AI, achieved by engineers, has speeded up their development over the past decade [15]. Moreover, because of their human-like shape, these robots can use the same equipment and environment as humans, hence, making them more compatible to be used as a building platform for the physical implementation of the Digital Twin.

These days, humanoid robots are available in various forms and dimensions and are extensively being used for research and space exploration, personal assistance and caregiving, education and entertainment, search and rescue operations, manufacturing and maintenance, public relations, and most importantly healthcare sector. Some of the several potential prototypes of humanoid robots that can serve the purpose are discussed below.

ASIMO (Advanced Step in Innovative Mobility) [16], [17] is one of the humanoid systems developed by Honda Motor Co. in the year 2000. Considered to be the world's most advanced humanoid robot, ASIMO uses Honda's new "I-WALK" technology to achieve a remarkable human-like ability to walk, climb stairs, hop on legs continuously, run backwards, and even walk over uneven terrain with high stability. However, the price for this advanced humanoid system is tagged at over 1 million USD, making it prohibitively expensive.

HRP-1, developed by Honda R & D [18], mainly for the maintenance task at the industrial plants and to provide security services for home and office costs about 400K USD. The more advanced and developed humanoid robot HRP-4 [19], is a life-size and has achieved a light-weighted body compared to its predecessors HRP-2 [20] and HRP-3 [21]. Although, this humanoid robot can coexist with humans in their living spaces, thereby improving their quality of life, it excessively priced costing approximately 50K USD. HOAP-1, a miniature humanoid robot [22] from Fujitsu, designed as an ideal tool for research and development in robotics technology also costs about 50k USD.

The work in [23] details another humanoid system -NAO Robot, developed by a French robotics company 'SoftBank Robotics', in the year 2008, with a motive to make the humanoid system affordable to more people. Because of its versatile nature, moderate size and human-like behaviour, the NAO robot is being used as an optimized teaching-aid tool for in-depth research on human-machine interaction, autonomous navigation, and cognitive computing, in numerous academic institutions worldwide. Besides its use in academia, the NAO robot is also employed in the healthcare industry to improve the standard of care provided and for efficient administration [24]. This robot is commercially available over a price range of 8k to 16K USD.

In [25] a child-sized 3D printed humanoid robot named HBS-1 is presented by the University of Texas, designed primarily for children's education and rehabilitation research, costing approximately 10K USD.

Inmoov [26], the first Open-Source 3D printed life-size humanoid robot, designed by French designer Gael Langevin, is another example of an economical humanoid robot, costing around 2K USD.

Some of the functional characteristics like the height, weight, body mass index, and degrees of freedom along with their manufacturing cost of the existing humanoid robots from literature are detailed in Table 2.1 below.

Table 2.1: Functional characteristics of humanoid robots

(BMI: Body Mass Index; NA: Not Available; *Manufactured using 3D printing technology, **More detailed information of DOF is not provided in the cited references)

Reference	Humanoid Robot	Height (h) (m)	Weight (w) (Kg)	BMI (Kg/m^2)	Degrees of Freedom (DOF)	Price (USD)
[17]	ASIMO	1.3	50	29.58	57 [7/arm(wrist); 13/hand] **	>1 million
[19]	HRP-4	1.51	39	17.10	34 [7/arm; 2/hand] **	250K
[22]	HOAP-1	0.48	6	26.04	20	50K
[23]	NAO	0.58	4.5	13.5	25 [5/arm; 1/hand] **	8K - 16K
[25]	*HBS-1	1.2	5	3.48	51[4/arm; 15/hand] **	10K
[26]	*Inmoov	NA	NA	-	NA	2K

From the above literature, it is evident that to have an economical humanoid robot, additive manufacturing technology should be incorporated in the design and fabrication of the humanoid robots.

2.2 Additive manufacturing of robotic hands

Additive manufacturing is a relatively new and progressively developing branch of technology, generally known as 3D printing. With the advent of this technology, prototyping and manufacturing of desired elements with the consecutive application of layers have seen a significant boost lately. This technology not only intends to provide relatively simple and cost-effective production of complicated 3D designs like anthropomorphic robotic hands which requires distributed sensors equipped within the structural design but also in making the general manufacturing and integration process of the system less complex and time-consuming.

3D printing can be defined as a technology that creates three-dimensional objects with one ultra-fine layer on the other. Each layer bonds to its preceding layer of melted or partially melted

building materials. The additive technologies employ various methods of fabrication. Of the many, Fused Deposition Modelling or Fused Filament Fabrication (FDM/FFF) is the most widely used method as it offers a low cost of production. This technique involves the extrusion of thermoplastic material like Polylactic Acid (PLA), Acrylonitrile Butadiene Styrene (ABS), Polyethylene terephthalate Glycol (PET-G), Nylon (PA-12), High Impact Polystyrene (HIPS), and Acrylonitrile Styrene Acrylate (ASA), through a heated nozzle. The dimensions of the type of polymers used in this process have been standardized as either 1.75mm or 3mm, with 1.75mm being more popular. We discuss in the next section 3D printed robotic hands that are already being used for several applications ranging from pick and place operation to realistic human-robot handshake.

The authors in the paper [27] present a 3D prinTable, six-axis anthropomorphic manipulator with only rotational joints as a robotic arm. The project of this manipulator is available under the Creative Commons Attribution-Share Alike 4.0 International (CC BY-SA 4.0) license. The design of this manipulator is modified as per the needs of the study and is printed using the FDM technology.

This 3D printed robotic arm can handle a maximum load of 0.75Kg and consists of a total of 54 prinTable parts that can be printed on any FDM printer with a printing area of 20x20x20cm. The maximum range of the robotic arm is about 62cm. The motion of this 3D printed robotic arm is controlled by seven bipolar stepper motors and the whole manipulator is mounted on the support structure for its stability. The authors were able to demonstrate a connection between Robotics Engineering and Additive Manufacturing technology by developing a cost-effective anthropomorphic robotic arm but with only rotational joints. However, for Robo-twin, a more human-like robotic hand with additional degrees of freedom is needed to make the overall human-machine interaction as close to real as possible.

Inspired from human hand anatomy, the researchers in [28], introduce a customized 3D printed robotic hand design to produce a genuine human-robot interaction. With a motive to imitate a human-like hand behaviour, the tailored robo-hand is attached on a Kuka LWR 4+ robotic arm having seven degrees of freedom. The prototype mainly focuses on achieving a convincing

finger grasping and palm compliance by implementing a position-controlled feedback loop. Most of the hand parts which are not exposed to relatively heavy forces but are complex in design were 3D printed using ABS plastic as a building material. However, the parts which experiences excess pressure from the human, like the hand's frame which holds the motors and the palm links, were made of aluminium for durability and robustness of the prototype.

One of the major limitations of this prototype that was studied from the results of the experiments is the lack of the fourth finger and better actuation mechanism for the thumb. It was also mentioned that the emulation of the human skin was not accurate. Although, the researchers were able to achieve palm compliance and finger grasping with a 3.7 rating out of 5 for comprehensive haptic rendering, the overall realism of natural human handshake was drastically affected.

[29] represents the design of a highly biomimetic and fully actuated 3D printed robotic finger capable of imitating the human finger not only in terms of phalanxes movement but also in the motion of tendon, bones, and ligaments of the human finger. This designed is inspired from the biomechanics of a human hand and allows a total of four degrees of freedom. The material used for 3D printing is rs-f2-gpcl-04, a type of clear resin with optical transparency and exhibiting the young's modulus of 2.8 GPa having a similar harness as that of human finger bones. Although, this finger design can mimic all possible gestures of a human hand, integration of sensors is not considered in its design which are vital for our application.

The authors in [30] put forward the design of a 3D printed soft robotic hand with integrated distributed tactile sensing in both fingers and palm, printed with an admixture of Vero and Agilus30 using multi-material polyjet technology. This hand can perform 32 Feix taxonomy grasps [31] out of 33 and all 11 Kapandji thumb opposition poses [32] demonstrating an agility that is comparable to a human hand. However, this design doesn't support any further integration of sensors for sensing temperature.

In [33] , the authors detail the development of a fully 3D printed capacitive sensor embedded entirely in the robotic hand to provide pressure sensing abilities. The capacitance-to-digital converter chip is also integrated within the sensor design. This integrated capability is achieved using innovative design and multi-material additive manufacturing technology. Firstly, a five-finger robotic hand inclusive of actuators (for the motion of fingers), is 3D printed using PLA as a building material. Secondly, to obtain a smooth pressure sensing phalanx, a fused filament fabrication printer having an extra printing nozzle for paste/ink printing is used to print the conductive and dielectric layers of the capacitive pressure sensor.

Different combinations of flexible dielectric and conductive materials were tested. The best performing pair of silver paint as a conductive material and soft rubber (Eco flex 00-30) as a flexible dielectric is used in the fabrication of the soft capacitive sensor because of their capability of efficiently recording low pressure values of 1kP a while exhibiting better sensitivity response with an average value of $0.00218 kPa^{-1}$. A linear response over the tested range of pressure values was demonstrated by this combination compared to other tested pairs.

Another reported advantage of this customized 3D printed robotic hand is the resemblance of the designed phalanx with that of the real humans. In this design the pattern of the bone surrounded with soft tissues and skin which forms the distal phalanx of human can be represented with a firm base made from black PLA as the bone, and the pair of flexible dielectric and conductive material resembling the soft tissues, and the uppermost layer of the TPU 3D printing filament as the skin. The top layer reflects the elastic properties of the human skin very closely by exhibiting a Young's Modulus of 12 M P a which lies in the range of the Young's Modulus of 5-20 M P a of the skin. The researchers were able to illustrate that the multi-layer additive manufacturing technique can be used to create robotic hands with integrated sensor providing more functionalities than conventional rigid robotic hands. However, this design is not compatible to integrate any other haptic modalities or sensing capability except pressure.

The research group at Nazarbayev University (NU) in [34] presents a preliminary prototype of a new semi-anthropomorphic multi-grasp robotic hand to serve as an end effector in industrial and

service robots. To maintain low cost and weight, and to have a relatively easy assembly, additive manufacturing techniques were widely used. Most of the hand's structure is 3D printed to keep its overall weight less than 1Kg, else the heavy weight of the hand will limit the payload capabilities of the base manipulator. The NU hand consists of 10 joints which are actuated by five tendons connected to four servo motors. Also, the rubber-like paddings on fingers and palm which are integrated into the design use 3D printing techniques. These paddings feel similar to the soft tissues present on human fingers and palms thereby helping in the conformal grasping of objects.

Besides, in [35] a 5-fingered anthropomorphic robotic hand is used to provide force feedback to the user through pneumatic haptic muscles on the glove. This robotic hand design is open-source 3D prinTable and is mostly used for research on prosthetic hands. The backside of the hand is printed in a black PLA material while the front palm and fingers are printed in gold Ninja flex, a flexible filament produced by Ninja Tek which gives the palm a softer texture thereby allowing for some compliance while grasping. The fingertips are embedded with soft force sensors for developing an intuitive teleoperating system based on IMU's where the user can move freely while the hand is still in operation.

Both prototypes in [34], [35] are suiTable to be used, but they are restricted to the use of one specific sensor and only offer the design of the wrist and not the complete hand i.e., the forearm, the bicep and the shoulder part.

In the papers [36], [37] the Inmoov (Open-Source 3D printed life-size humanoid robot) design of both hand and arm is used. The researchers in [36] modified the Inmoov design using CREO Parametric 3.0T M to incorporate both temperature and pressure sensors inside the fingertips. A layer of silicone covers these sensors and some other parts of the hand to provide stronger gripping capability and a more human-like appearance. Acrylonitrile Butadiene Styrene (ABS) material is used to print all the hand and the arm parts on a Fortus 3D printer, with a total volume of 78in3. The printed hand is about the same size as of a male human's hand with forearm being a little longer and wider to accommodate the standard sized servo motors. In [37], a wireless-

controlled 3D printed robotic hand system consisting of a gesture control glove and a 3D printed Inmoov forearm is demonstrated. The forearm with a total of 46 individual parts was 3D printed with white biodegradable polylactic acid (PLA) material, for its low printing temperature and smooth printing finish. The forearm replaces the use of human hand to do dangerous tasks remotely, with each finger consisting of three rotational joints.

To be useful for daily tasks, the hand of the Robo-Twin requires the use of various sensors (temperature and pressure) to have more than one haptic modality. Hence, the 3D printed design of the robotic hand should be able to incorporate this very vital need. With most of the available hand designs being restricted to only one specific sensing functionality, the open source Inmoov design of the robotic hand seems to be the best available option as the design can be easily customized.

Another aspect is reducing the cost of an anthropomorphic robotic hand, using under-actuated mechanism techniques, i.e., using fewer actuators than the degrees of freedom. It not only makes the system less complex but also reduces its cost to a greater extent. However, the human hand can perform complex tasks while retrieving information from the surrounding environment. This is the grasping organ of the human body which uses approximately 29 bones and 34 muscles to move all the fingers [38]. Due to such a high degree of freedom and massive neural connections the human hand can produce all kinds of finger movements like pinch, grasp, touch, squeeze, throw, and hold while demonstrating immense flexibility. Therefore, it is very important to select the appropriate under-actuated mechanism to reflect, as closely as possible, the enormous flexibility of the human hand while reducing the cost and complexity of the system.

2.3 Underactuated designs

A highly under-actuated design of a robotic hand is discussed in [28], wherein only two electric motors (namely finger motor and palm motor) are used to control the entire motion of the hand. The mechanical design of the robotic hand consists of three fingers and one thumb. The motion of all fingers is obtained in a similar manner as tendons in the human hand. The finger motor provides a maximum of 111N of force. This force is connected to a parallel slider bar, used for

equally distributing the force to the finger cables attached to it. This force distribution technique is used to achieve a homogeneous grasp as each finger should apply an almost equal amount of force on the opponent's hand while making a handshake. The slider bar is actuated by the finger motor to move towards it along the guiding rods while pulling in the attached finger cables thereby making the hand grasp. The palm bars are attached to a simple pin joint which provides a systematic palm motion with two degrees of freedom. To synchronize the system, a gear wheel is used to interlock the palm bars. However, it was observed that the palm mechanism is not capable of transmitting a minimum required force of 50N to the palm (compared to its calculated force of 17.3N). To overcome this, rubber pads of dimension 15mmX25mmX10mm with a shore hardness of 40A are placed between the palm bars. These rubber pads absorb the additional compressive forces and exhibit a similar elastic hysteresis behaviour as observed in the human palm.

Although his highly under-actuated design of the robotic hand is able to provide a similar force distribution contributing to human-like haptic feedback and making the grasp of the handshake fully self-adaptive, a lack in the grasping strength and a longer duration in making a handshake with a human subject was observed.

The paper [39], illustrates an improvised version of the under-actuated mechanism of the robotic hand in [28]. The prototype in [28] uses the motors beyond their load limit leading to overheating and the shaft was not able to be doubly supported because of the use of parallel slider bar mechanism. Therefore, in [39] the actuators were replaced to provide the required forces and operated within their respective limits and both the geometric centre and the centre of mass are kept relatively closer by fixing the motors on either side of the hand as compared to the same sides in [28] . Also, some of the structural components are made up of aluminium in [39] to avoid wear and tear of the plastic printed components as in [28] .

The fingers are actuated in a similar manner as described in [28], except that the current prototype's thumb is redesigned to provide 2 DOF rather than 1 DOF. It is not set in motion by the motor, instead it is passively driven by the palm's compression. This is done by connecting

its string to the opposite finger than to the slider bar. As a result, the compressive force applied by the thumb on the human hand is depended on how strongly the palm is compressed.

The design of the lever proposed in [28] to achieve the motion of the palm is also improvised. Instead of utilizing three bars arrangement to connect the levers to the middle finger, it now uses a two bar and a cylindrical guide system resulting in the linear motion of the middle finger by always having it on the symmetric axis between the two levers. Also, the disk and bar mechanism in [28] to transfer the middle finger motion to the motor tends to reach a singularity, this is avoided by replacing it with a simple cable and pulley system. The major drawback of this under-actuated design is the inability of the thumb to produce an adequate natural grasping effect because of its passively driven motion.

In [40], the robot Vizzy, a four-fingered robot, is used to carry out a study of the handgrip strength for comforTable handshakes. The thumb and the index finger are controlled by a single motor while the middle finger and the ring finger are connected to another motor. A pulley is attached to the motor of a finger, and a fishing line string runs through it to the last joint in the finger. Hence, the motion of the motor causes movement in all three joints of the finger. Although the robot Vizzy follows an under-actuated mechanism, a detailed description of such is not mentioned.

A Tendon-Pin Under-actuated (TP-UA) mechanism of Columbia Hand is discussed in [41]. The Columbia Hand consists of 3 fingers having 3 degrees of freedom each, and are actuated with only two motors, one for closing the fingers and the other for rotating the thumb around its base. In order to compensate the missing DOF’s, a number of sensors has been integrated in the hand design that can evaluate the joint angles and tactile contacts on each part of the hand.

In TP-UA, every part of the robotic finger relates to pin joints and a tendon with the response being studied in three different stages while grasping an object, I.e., the Initial stage, Pre-Shaping stage, and the Closing stage. In the Initial stage, the finger is in straight position by means of return springs and the tendons running through every segment of the finger with the

other end connected to the actuator. During the Pre-Shaping stage, the finger will start closing because of the tensile strength applied by the actuator on the tendon, simultaneously rotating the joints in a coupled relationship. Finally, in the Closing stage, the middle phalanx is blocked, and the tendon is still being pulled down by the actuator while the distal phalanx continues to bend. The joint angle between the two is decoupled by the object.

One of the advantages of using this under-actuated mechanism is that it can complete the grasp task with the use of a single actuator with minimum number of lifting mechanisms as used in other under-actuated mechanisms.

In [34], an under-actuated design of NU hand is detailed. This hand consists of 10 joints, actuated by 5 tendons connected to 4 servo motors. The to and fro motion of the thumb is achieved by connecting it directly to the micro servo motor. The second joint of the thumb is controlled by a digital brushless servo motor (Futaba BLS153). The motion of index finger is realized by connecting it to a standard digital servo motor (HITEC HS322). Finally, the motion of the rest of the three fingers are controlled by one servo motor (HITEC HS322) via differential coupling, i.e., by distributing the applied force between the three fingers using elastic elements. The elastic elements used in the design acts in series with tendons and are 3D printed using Object Connex 260 printer. The curling motion of the fingers is achieved by means of tendons while the torsion springs are used to release the fingers back to their normal state.

A 10 degree of freedom NU Hand is actuated with only four servo motors. Hence, the highly under-actuated design allows the fingers to perform conformal grasping without the need of any addition actuator.

The 3D printed, 5-fingered anthropomorphic robotic hand in [35] employs four linear actuators, namely Actuonix PQ12-R, to achieve the motion of its fingers, one for each first, second and third finger and the remaining one for both fourth and fifth finger. Although the design of the robotic hand is under-actuated, the mechanism used to achieve the under actuation is not discussed.

In both [36], [37] the phalanxes of each finger i.e., the distal, middle, and proximal phalanxes are controlled with only a single actuator making it a highly under-actuated design. The actuator used in these phalanxes is HS-35HD Hi-tech servo motor, placed inside the forearm. The plastic servo horns that come with the servo motors are replaced by 3D printed servo pulleys through which a fine braided fishing line is passed. This braided fishing line makes it way to the fingertips after running through holes integrated within the design, acting just like the tendons in the human body. At the servo end, the string is wound around the servo pulley and tied at one of its edges such that when the servo is operated, it rotates, and the string is pulled further to its edge thereby causing the fingertip to move in towards the palm. Springs presented in each finger joints add to the smooth and more controlled motion of the finger.

Therefore, the tension in the string causes the distal phalanx to bend inwards. As the tension keeps on increasing due to the torque provided by the servo motor, the middle phalanx followed by the proximal phalanx curls in too. Hence, the curling motion of the finger which constitute 3 DOF is achieved by making use of only one actuator. Fingers are returned to their normal resting position by just rotating the servos in the opposite direction by the same amount/angle.

However, to achieve better grasping motion, two servos are used to control the motion of the thumb. The extra servo is used to directly drive the thumb in a plane same as that of the palm of the hand and its closing motion is achieved in the same manner as the rest of the four fingers. This under-actuated mechanism is used in the Inmoov hand design of the robotic hand.

2.4 Temperature Sensors

The research in [36] uses the temperature sensor PT502J2, a 10K thermistors from US Sensors in their robotic hand for temperature measurement. This small size, low cost, highly accurate and sTable device is designed especially for temperature sensing and control applications where it is necessary to eliminate the expensive individual circuit calibration to make the overall process cost-effective. Operating in the range of −80°C to +150°C with an accuracy of ±0.2°C, it provides fast thermal response time with a thermal constant of maximum 1 second and a dissipation constant of 1mW/◦. For better-grasping capability these sensors were covered with a layer of

silicone elastomer of 0.05−0.07 inch thick. Although silicone is known to be a heat resistant material, the overall impact on the performance characteristics of the thermistors was found to be less effective. For example, the time constant of the thermistors with and without silicone covering was observed to be 16.5 seconds to 15 seconds respectively with a reduction of 2°C in its steady-state temperature value.

Initial testing of the temperature sensor indicated that the hand could identify hot objects. However, during the sensing test, it was found that the cooling rate of the temperature sensors was rather slower.

The design and fabrication of a liquid metal-based wearable tactile sensor capable of measuring contact forces and temperature independently is presented in [42] . This sensor is designed to be worn on an index finger and thumb of the human hand for the measurement of tactile information while grasping an object. A proper balance between temperature and force sensing is achieved by employing the Wheatstone bridge circuit.

Among a variety of available liquid metals, Galinstan (gallium-indium-tin) is used in the fabrication process because of its wide temperature range (low melting point of −20°C and a very high boiling point of 2300°C), high surface tension ($718X10^{-3}$N m^{-1}), low viscosity ($2.4X10^{-3}$ Pa.s), high electrical and thermal conductivity ($3.46X10^{6}Sm^{-1}$ and 16.5W $m^{-1}K^{-1}$). Galinstan was then filled in fingerprint-shaped fluidic channels and oval-shaped bulges enclosed in an elastomer structure made up of Polydimethylsiloxane (PDMS) providing excellent flexibility, easy operation, and better skin contact.

The temperature sensing sensitivities are calibrated to $0.41\%°C^{-1}$ from 20°C to 50°C and to $0.21\%°C^{-1}$ from 50°C to 80°C. Grasping experiment of water-filled beaker demonstrated that the developed sensor is capable of accurately measuring contact temperatures and can be reliably used in tactile sensing applications.

In [43] a small passive EPCOS fast response 10K NTC thermistor is used to estimate the surrounding air temperature before and during the contact with the object. It is then incorporated within a handheld porTable device with tactile sensing modalities to have a data-driven thermal recognition of contact with people and object.

The paper [34] highlights the use of Melexis MLX90614, as a contact-less infrared temperature sensor, housed inside the sensor module placed on the NU hand to provide autonomous intelligent object manipulation capability to the robotic hand. This non-contact temperature sensor prevents the NU hand from avoiding contact with hot objects. However, the papers [34], [43], does not detail the thermal characteristics of the temperature sensors used while performing grasping and sensing tests.

[44] details the manufacturing of a printed skin alike temperature sensor with Poly (3,4-Ethylene Dioxy Thio-phene) Polystyrene Sulfonate (PEDOT: PSS) and Graphene oxide as a composite material and silver as contact electrodes. The layer of the composite material used exhibits sensitivity towards temperature. To illustrate the temperature sensing test of this printed temperature sensor, it was then placed on the distal phalanx of the thumb of a 3D printed robotic hand and then placed over a heating arrangement. Upon reaching a set threshold value, the finger is moved away from the hot object, actuated with a linear servo motor placed inside the palm region.

To demonstrate its reliability for temperature measurement applications, the performance characteristics are compared with RS PRO Thermistors DO-35 100KΩ, a commercially available thermistor. Both these temperature sensors were placed on the hot plate at room temperature while gradually increasing the temperature of the hot plate to 100°C. The printed temperature sensor showed high sensitivity towards temperature changes with around 80% change in resistance at 100°C with a response time of 18s in comparison to 90% change in resistance at 100°C with a response time of about 65sec as demonstrated by the commercial thermistors. Also, the recovery time of these sensors are evaluated by allowing them to cool down to room temperature after removing from the hot plate. From the recovery paths plotted for

both, the printed sensor recovered completely after 32 seconds compared to 120 seconds taken by the commercial thermistors.

Therefore, it can be concluded that the printed skin like temperature sensor showed a faster response than the used commercial thermistors and is a promising solution to be used in Eskin [45] applications in humanoid robots. However, this printed sensor demonstrated more response time than the PT502J2, a 10K thermistors from US Sensors used in .

The paper [46] presents the design of a low-cost robotic finger with soft fingertip, having position, temperature, normal and shear force sensors, entirely embedded inside the design to be used in the new version of humanoid robot ARMAR-6. The sensory system employs four 3D shear force sensor which consists of a 3D Hall effect based digital sensor (MLX90393, Melexis) with their corresponding magnets cast in silicone rubber and two normal force sensors. Although both pressure and hall effect sensors can measure the temperature of the object or material it is in contact with, pressure sensors provide more accurate and reliable thermal information.

To assess the response of the sensor to thermal flux, four different materials, I.e., wood, PVC, steel, and aluminium were placed inside the freezer at −20°C. After the immediate removal of these materials outside the freezer, their temperature was measured by placing one of the pressure sensors on the finger in direct contact with the material while the temperature was allowed to cool down to room temperature. The Wood showed minimal impact on the temperature measured by the sensor because of its low thermal conductivity while steel demonstrated the highest impact. Hence, the fingertip can differentiate various strengths of thermal flux within seconds and identify high-temperature surfaces.

The construction of a vision based soft somatosensory system for tactile modalities is discussed in [47]. In this, a transparent coating of Thermochromic Liquid Crystal (TLC) Ink is used on the finger-shaped sensing surface. TLC is sensitive to temperature changes as the distance between its molecules vary once the temperature starts changing within its working range. As the distance changes it reflects different wavelengths of light. On the colour spectrum, it varies from red to

purple of the visible spectrum of light when the temperature goes from lower limit to higher limit of the operating temperature range of TLC ink.

To evaluate its accuracy in measuring temperature, the sensor is placed inside the oven and heated from 25˚C to 31˚C. The images of colour variation during this process as well as the corresponding real-time temperature are recorded using a camera and a reference thermometer respectively. The captured images are then converted from RGB to HSV colour space to avoid lighting interference while measuring the TLC colour. It is observed that the hue values of the reflected light increase while its wavelength decreases. Therefore, a linear relationship between the hue values of the reflected light from the TLC ink and the estimated temperature is established.

From the test results obtained, it is concluded that the temperature sensing range of this sensor is from 25˚C to 31˚C with a temperature estimation resolution of 0.4˚C I.e., 6.7% of its sensing range. However, to employ this sensor in robotics applications such as anthropomorphic robotic arm, its small sensing range becomes one of its major drawbacks.

The temperature sensors and some of their functional properties discussed above are summarized in the Table 2.1.

Table 2.1 Functional properties of studied temperature sensors

Papers	Type of Temperature Sensor	Working Principle	Operating Range	Accuracy of measurement	Thermal Constant	Dissipation Constant	Time Constant	Temperature Sensing Sensitivities	Response & Recovery Time
[36]	PT502J2 10K Thermistor	Thermistor	-80°C to +150°C	±0.2°C	1s max	1 mW/°C.	15s	N/A	N/A
[42]	Wearable Tactile Sensor	Galinstan Liquid Metal-based	20°C to 2300°C	N/A	N/A	N/A	N/A	0.41%°C^{-1} from 20°C to 50°C and to 0.21%°C^{-1} from 50°C to 80°C	N/A
[43]	Passive EPCOS 10K NTC	Thermistor	N/A	N/A	N/A	N/A	N/A	N/A	N/A
[34]	Melexis MLX90614	Infrared	-40°C to +125°C	N/A	N/A	N/A	N/A	N/A	N/A
[44]	Printed Temperature Sensor	PEDOT: PSS & Graphene Oxide Composite	25°C to 100°C	N/A	N/A	N/A	N/A	1.09%°C^{-1}	18s & 32 s
[47]	Vision based soft somatosensory system	Variation in temperature properties of Thermochromic Liquid Crystal	25°C to 31°C	0.4°C	N/A	N/A	N/A	N/A	N/A

The breakdown of temperature sensing technologies used in the above research studies is represented in the Figure 2.1 below.

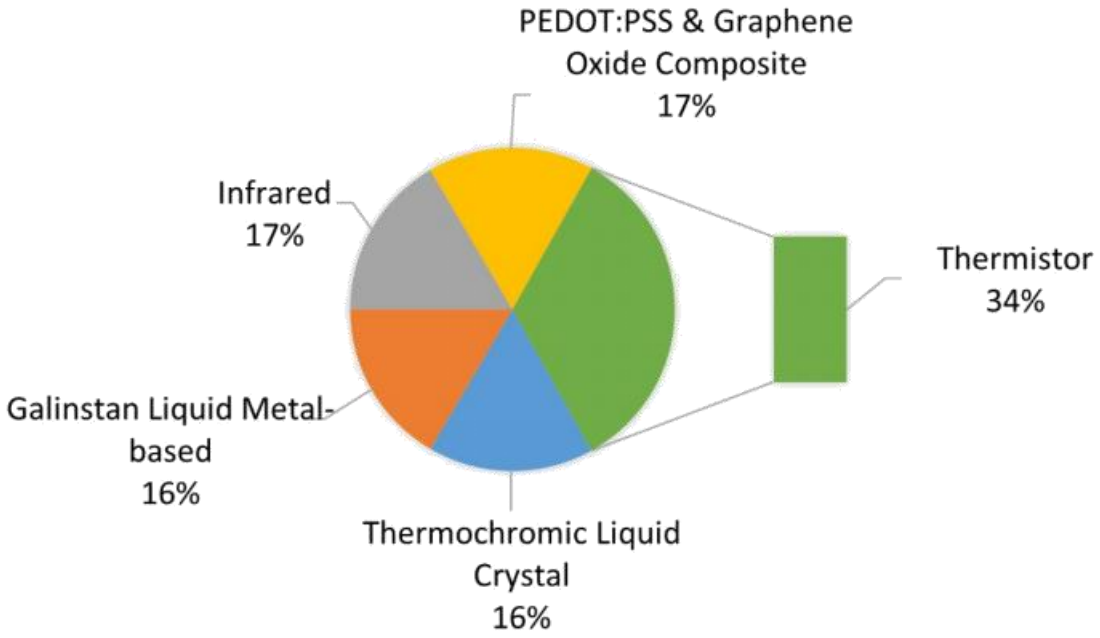

Figure 2.1 Breakdown of temperature sensing technologies used in the literature

The pie-chart above indicates that thermistor-based sensing technology is the most widely used method in determining the contact temperature in any application involving a robotic hand. Hence, the choice of thermistor as a temperature sensing technology in our application.

2.5 Pressure Sensors

The research work in [36] uses A101 Flexi Force sensor to measure the applied pressure because of its small size, low cost, high durability, and easy implementation. Pressure sensors were placed on the fingertips for achieving maximum sensing capabilities, inspired by the work presented by Mirkovic and Popovic in [48]. Therefore, the sensors are incorporated into the distal phalanxes of each finger.

However, using one sensor per fingertip imposes a difficulty to measure the applied force on any part of the fingertip as the sensing area of the sensor is only 0.15 inches. To overcome this problem, a cantilever beam is designed and placed hanging over the sensor's surface. This

cantilever beam concentrates the applied force anywhere on the fingertip to the sensor's center, thereby increasing the sensing area of the sensor. The results obtained from the grasping test performed by the hand demonstrated that it could grasp various objects of different shapes and sizes and the corresponding pressure sensor readings were plotted for each fingertip. The sensors responded readily to the change in the pressure values.

Research in [40] uses tactile sensors made up of soft elastomer body consisting of a 3-axis Hall-effect sensor placed below a small permanent magnet inside it. On the application of external force on the elastomer, the relative position of the permanent magnet changes. This variation in the magnetic field is detected by the hall-effect sensor and is proportional to the applied external force. 3-axis Hall-effect sensor detects the magnetic field variations in 3 axes, allowing the tactile sensor module to measure the magnitude and direction of force in 3 dimensions. These sensors have the capacity to detect minimum forces in the order of 10mN.

Experiments were conducted to analyze the qualitative feedback from human subjects while they make a handshake with robot Vizzy (a four fingered humanoid robot). A total of 15 tactile sensors are placed on the robot's hand with 3 on thumb and 4 on each of the other fingers. The given placement of sensors yields the force distribution on several contact points rather than just fingertips. As a result, many of the human subjects reported experiencing more comforTable handshake than expected. However, they reported that the length of the hand is slightly larger than normal and recommended to have same tactile sensing feeling in the palm as in the fingers.

In paper [41] a highly under actuated design of Columbia Hand with integrated joint angle and force sensors is presented. In this, a Force Sensitive Resistor (FSR) is used as a force/pressure sensor because of its low cost and relatively high sensitivity compared to capacitive tactile sensors and piezoelectric polymer films. Although FSR is a nonlinear device which is highly sensitive to changes at low forces and much less sensitive to changes at high forces, a voltage divider with nonlinear transfer characteristics is employed to provide greater values of output at smaller values of sensor's resistance.

In this, FSR's are only used to determine whether the Columbia Hand is in contact with an object or not by setting a reference voltage. No more details on the pressure/force sensing capacity of the hand are provided in the paper.

The development of a complex 3D printed robotic hand with an integrated soft capacitance touch/pressure sensor having dimensions 19.6mm wide, 2.6mm thick, and 28mm high is presented in [33]. The phalanxes are designed with gaps to house the electronics related to and the pressure sensor. A total of five different capacitive pressure sensing phalanxes were fabricated with a combination of conductive and dielectric materials, namely Eco flex-silver (Eco-Ag), Eco flex-graphite (Eco-Grp), Eco flex-conductive PLA (Eco-PLA), thermoplastic polyurethane-silver (TPU-Ag), and thermoplastic polyurethane-graphite (TPU-Grp). All these five devices are tested not only for their sensing capabilities under a constant pressure of 20KPa for 8 mins but also for hysteresis and dynamic cycle response with increasing pressure from 0KP a to 50KPa.

The pair of silver paint as a conductive material and soft rubber (Eco flex 00-30) as a flexible dielectric is used in the fabrication of the soft capacitive sensor not only because of their capability of reliably sensing pressures as low as 1kP a while exhibiting better sensitivity response with an average value of $0.00218kPa^{-1}$ but also for demonstrating a linear response over the tested range, compared to other four pairs. Although the authors have demonstrated a simple and cost-efficient method for a pressure sensing system, this 3D printed hand is only capable of sensing pressure. Moreover, the design is not compatible to adapt the addition of extra sensors for measurement of other physical parameters such as temperature in our case.

A variety of methods are described in the literature of [49] for the measurement of contact forces between the human fingertip and an object. A strain gauge as a force sensor attached to the object, allows accurate measurement with high resolution. The only limitation is that for every different object a custom-made device must be developed and calibrated for conducting experiments. The process become laborious with the increase in number of objects.

A force sensitive resistor can be placed on the fingertip to measure the contact forces. Although FSR provides advantages of low cost, small thickness, and flexibility, the major limitation is the lack of sense of touch as the sensor comes in between the human fingertip and the object. Moreover, its non-linearity, drift, saturation, and hysteresis makes it difficult to be used in custom-made solutions.

Another proposed method is to examine the colour changes of the fingernail while making contact with different contact forces. This way the user will not lose the haptic sense as the finger is in direct contact with the object. Nevertheless, the limitations are prominent, as the result changes drastically from one person to other and the calibration process is grueling.

Lately, some researchers have proposed to measure the change in the width of the finger caused by the normal deformation force of the finger pad while contacting an object. This change can be measured by a sensor placed at the side of the fingertip, thereby, eliminating the use of sensor between the fingertip and an object. This will provide the whole haptics information to the user grasping the object.

In [50], tactile data is obtained using JACO arm (a product of Kinova Robotics) equipped with Tekscan tactile sensor. This sensor consists of 18 segments to be connected to fingers and different regions of the palm. The Tekscan Grip system for R & D is used to obtain data related to pressure distribution while grasping an object over a 10 second time interval. Grip Research 6.70 is the software that converts the output voltage of the resistive sensor elements into relative pressure values in pounds per square inch (psi). Though a 95.21% of classification accuracy with a processing time of 2.6166 seconds is achieved in identifying different objects using the acquired pressure data, this sensor is designed only for thumb, ring finger and little finger of the human palm.

The mathematical analysis and fabrication of a cost-effective, flexible, aluminum-coated, polyimide paper based, touch mode capacitive pressure sensor is described in [51]. This fabricated pressure sensor is tested in all four regions of its operations demonstrating highest

sensitivity in touch mode operation from (10 to 40) kPa of exerted pressure compared to the normal mode (0 to 8) kPa, transition mode (8 to 10) kPa and saturation mode (after 40kPa) operations with a response time of 15.85 ms.

The MEMS-based capacitive pressure sensors offer various advantages over Piezoresistive pressure sensors such as high stability, low power consumption, high pressure sensitivity and repeatability, and low temperature drift. However, they require large diaphragm area, and has low dynamic range and exhibits non-linear response. The touch based capacitive sensors not only overcome these drawbacks but also, they offer less separation gap between the electrodes at high-pressure values. Because of their linear response, touch-based capacitive sensors can be efficiently used in making cost-effective skin-like material for prosthetic hands.

As mentioned earlier, the liquid metal-based wearable tactile sensor in [42] is capable of measuring both the contact forces and the temperature independently. The Wheatstone bridge circuit helps in decoupling the force and temperature signals. The force sensing sensitivities is calibrated to $0.32N^{-1}$. Grasping experiment of water-filled beaker demonstrated that the developed sensor is capable of accurately measuring contact forces and can be reliably used for multi-mode tactile sensing in real applications.

A single 2.5cm square of a stretchable fabric-based force sensor is used in [43] , the raw ADC output of which is converted in Newtons assuming uniform pressure distribution over the fabric. However, authors didn't discuss the functional aspect of this fabric-based pressure sensor in detail.

The design of a low-cost robotic finger with soft fingertip, and position, temperature, normal and shear force sensors, entirely embedded inside the design to be used in the hand of a new version of humanoid robot ARMAR-6 is discussed in [46]. The sensory system employs four 3D shear force sensor which consists of a 3D Hall effect based digital sensor (MLX90393, Melexis) with their corresponding magnets cast in silicone rubber and two normal force sensors. The experiment results demonstrated that the pressure sensors showed higher sensitivity to pressure

than the Hall-Effect sensors, but they get saturated at high pressure values greater than 126 kPa, while the Hall-Effect sensors continued to respond. Therefore, this combination of sensors for pressure measurement not only provides higher sensitivity but also wider range of measurement, thereby utilizing the benefits of both the sensors. The placement of these sensors allows forces over the whole area of the fingertip to be determined.

However, this combination imposes a complexity in maintaining a balance between signal clarity and mechanical benefits during grasp action as the tactile sensor signals are influenced by material creep induced by using a flexible material with a less ShA hardness.

The functional properties of the above-mentioned pressure sensors are summarized in the Table 2.2 below.

Table 2.2 Functional properties of studied pressure sensors

Papers	Type of Pressure/Force Sensor	Working Principle	Force/Pressure Resolution or Range	Force/Pressure Sensitivities	Curve Characteristics	Response Time	Saturation level
[36]	A101 Flexi Force	Force Sensitive Resistor	N/A	N/A	N/A	N/A	N/A
[40]	3-axix Hall Effect Sensor	Magnetic Field variation	10 mN	N/A	N/A	N/A	N/A
[41]	Force Sensor	Force Sensitive Resistor	N/A	N/A	Non-Linear Response	N/A	N/A
[33]	Soft Capacitance Touch Sensor (Silver paint and Eco flex 00-30 based)	Capacitance variation	1kPa	$0.00218kPa^{-1}$	Linear response	Few 100 ms	N/A
[50]	Tekscan Tactile sensor	Force Sensitive Resistor	N/A	N/A	N/A	N/A	N/A
[51]	Flexible touch-based pressure sensor	Capacitance variation	(10 to 40) kPa	N/A	Linear response	15.85 ms	N/A
[42]	Wearable Tactile Sensor	Galinstan Liquid Metal-based	0 to 13.5 N (0 to 54 kPa)	$0.32\ N^{-1}$	Linear response	N/A	N/A
[46]	3D Shear force sensor (MLX90393, Melexis)	Hall effect	50 grams	N/A	N/A	N/A	>44N (126 kPa)
[46]	Normal force sensor	MEMS Barometer	0.5 grams	N/A	N/A	16.5 s less**	0.1 N - 44 N (100kPa - 126kPa)

The breakdown of pressure sensing technologies used in the literature is represented in the Figure 2.2 below.

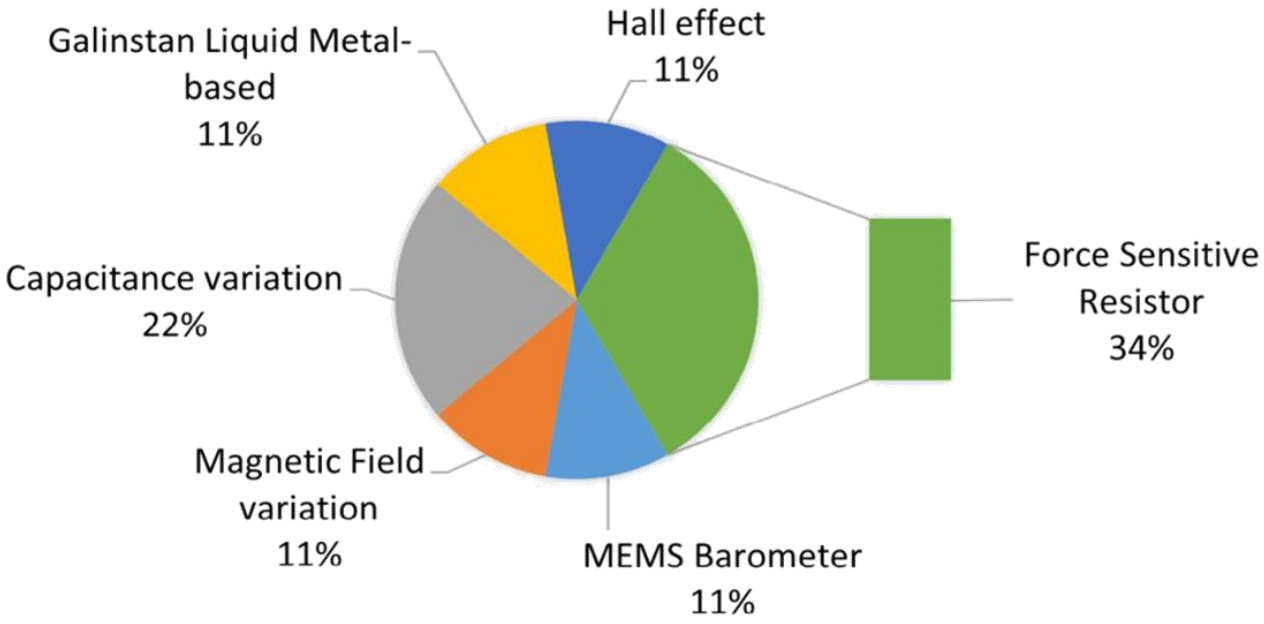

Figure 2.2 Breakdown of pressure sensing technologies used in the literature

The pie-chart above indicates that force sensitive resistor is the most widely used method in determining the contact force in any application involving a robotic hand. Hence, the choice of force sensitive resistor as a force sensing technology in our application.

3. Design of Robo Twin Arm

This chapter discusses the overall requirements and methodology of our proposed representation of Digital Twin's robotic arm along with its system's architecture for imitating a human handshake consisting of various modules discussed in detail.

3.1 Requirements of the Proposed System

This section discusses the set of requirements for our proposed Digital Twin's robotic hand for handshake based on the objectives stated in section 1.2 and in light of the related work presented in Chapter 2. We identify the characteristics that we feel would make the robotic arm more interactive and provide human alike feeling while making a handshake. From the studied literature, the following are the most important requirements for accomplishing our goals.

- ✓ **Design:** 3D printing technology has been found by researchers to be a promising solution in reducing the cost of DT representation, making it affordable to the public. The Robo-Twin hand requires the use of various sensors to have more than one haptic modality to be useful in assisting in day-to-day tasks. However, most of the hand designs available in literature are restricted to only one specific type of sensor. We found that the Inmoov design of the robotic arm to be the best available option as of now, as the design can be easily customized to incorporate both sensors and actuators.

- ✓ **Sensing and Actuation:** Apart from just demonstrating high flexibility in producing various finger movements, the human hand carries out a variety of functions with sensory and motor being among the most important ones. Both sensory and motor functions of the human hand make it an important organ as they help in collecting information and carrying out some daily tasks. Therefore, the DT robotic hand must be able to carry out some of the sensory and motor functions of the human hand. With temperature and pressure sensing being important senses to humans, the Robo Twin's hand should incorporate at least temperature and pressure sensors making it capable of sensing the physical temperature and pressure of the contact subject or the surrounding environment.

- ✓ **Placement of Sensors & Actuators:** There is a scarcity in research analyzing the sensors placement on the robotic hands. Be it temperature sensors or pressure sensors, we did not find in the papers surveyed much information on the choice of the placement of sensors. We believe however that this has potential to make a difference in the accuracy of the measured and reported temperature and/or pressure, depending on the application. In the example of the handshake, different parts of the palm and the back of the hand are pressed to different extents, and different parts are more/less sensitive to temperature. Hence, the choice of the sensory placement is of high importance in our application of a robotic arm for making a handshake with real humans.

- ✓ **Data collection and handshake replication:** One of the most important aspects of our proposed system is the collection of DT robotic hand's sensory data over the USART communication protocol. However, the dearth in the associated research has led to several potential research questions that needs to be considered to provide more insights towards the design and development of the DT robotic representation. Few of the gaps highlighted by the researcher in this aspect are as follows:

    - ✓ Whether the captured sensory data need to be compressed for effective storage and transmission? If yes, how will this be achieved?
    - ✓ Following the DT robotic hand's sensory data to achieve a virtual handshake, what is the best way to reproduce this handshake remotely, and how accurate will the handshake replication be?

For the purpose of proof of concept, our proposed Robo Twin system should be able to at least record the sensory data in real-time and transmit it using any of the existing communication protocols, to actuate the actuators for the user to sense force/pressure feedback.

3.2 System's Overview

The main idea of the proposed concept of Robo Twin is to allow two individuals say Real Twin A and Real Twin B, to perform a handshake as illustrated in the Figure 3.1. To be able to achieve this we designed two right-handed Robo Twin arms, both integrated with temperature and pressure sensors and vibrotactile pressure actuators to sense and actuate on the handshake data.

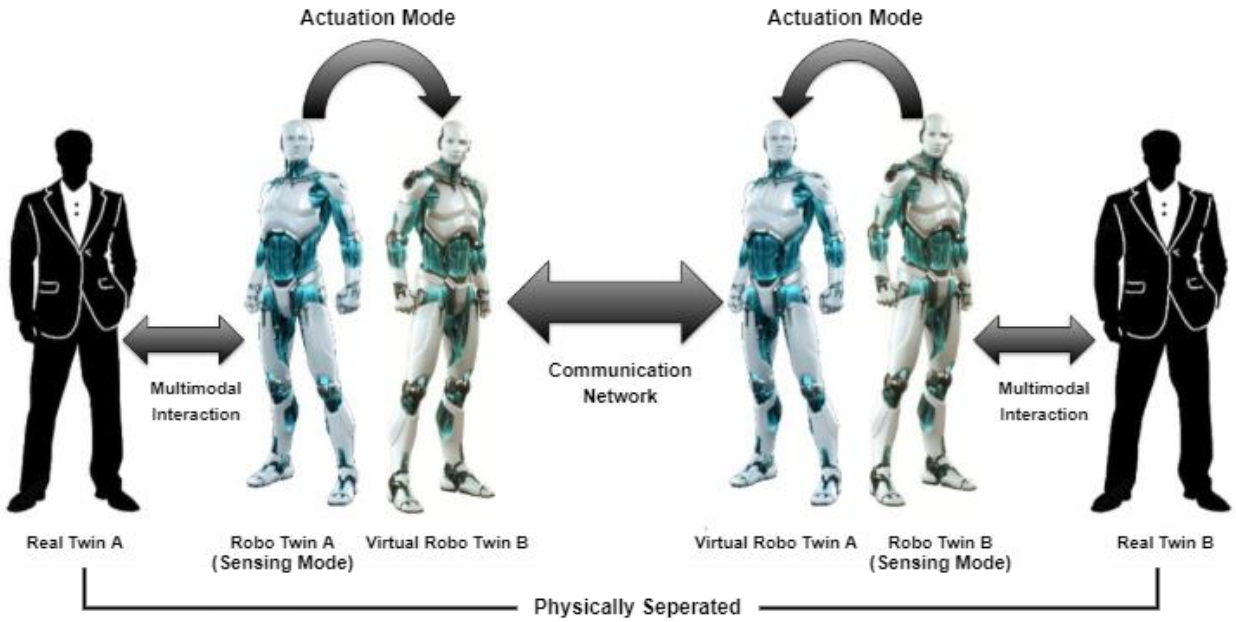

Figure 3.1 Proposed concept of robo twin

In sensing mode, both Robo Twin A and Robo Twin B will sense the handshake data from Real Twin A and Real Twin B respectively and then simultaneously exchange the sensed data to provide input data to the actuators to act upon in the actuation mode. It is very interesting to note that, when the Robo Twin is in its actuation state, it will act as a virtual copy of the other connected Robo Twin, representing the physical state of the Real Twin on the other side. To simplify, when Robo Twin A goes in the actuation state providing feedback based on the sensed data received from Robo Twin B over the communication network, it is acting as a virtual copy of Robo Twin B so that the Real Twin A feels the physical state of Real Twin B and vice versa.

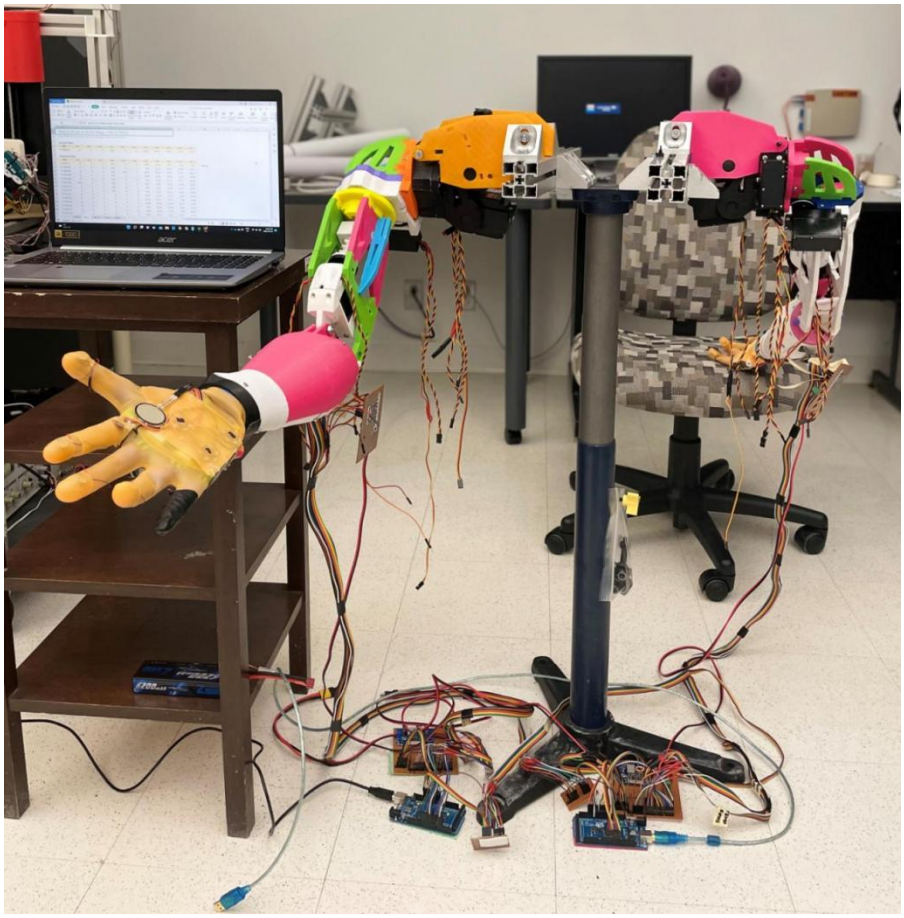

Figure 3.2 Two right-handed robo twin arms mounted on a 3ft pole on either side

These two right-handed arms are then mounted on a 3ft pole, one on each side, as shown in the Figure 3.2, with each arm having its own microcontroller for collecting, transmitting, receiving, and processing of sensed data. The sensory data is then bidirectionally transmitted between the Robo Twin arms using an existing USART communication protocol to actuate the vibrotactile pressure actuators, providing the user an accurate force feedback as being applied by the other user on the other hand.

3.3 System's Architecture

In this section, we provide an overview of the overall systems structure. Figure 3.3 shows the architecture of the Robo Twin system including its associated modules, namely sensing, processing, data collecting and data transmitting and receiving.

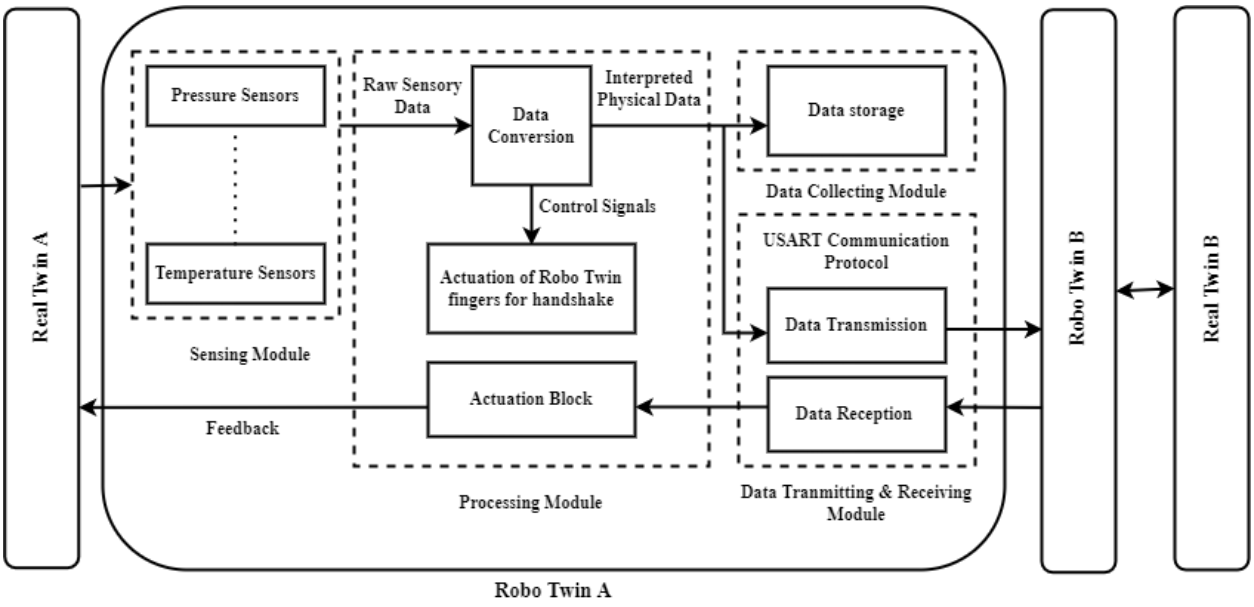

Figure 3.3 Robo twin system's architecture

The sensing module senses the warmth of the hand and the fingertips, and the force applied by various areas of the user's hand while performing a handshake. This sensed data is then passed to the processing module where it gets converted to interpreted physical data and sent to the data collecting module for its real time recording. Another important task of the processing module is to actuate the servo motors of the fingers for handshake motion and actuating the corresponding vibrotactile actuators. The simultaneous and bidirectional transmission and receiving of data across two Robo Twin hands is handle by the data transmitting and receiving module using existing USART communication protocol. These modules and their functionalities along with their workflow are described as follows.

1. Sensing Module

This module is activated as soon as the system is powered on. The main duty performed by this module is to sense the raw sensory data from the real twin while the Robo Twin hand is in contact, performing a handshake. All the raw signals received from the sensors are then sent to the processing module where they gets converted to their corresponding physical values by the controller.

This sensing module's workflow is represented by the means of a flowchart in the Figure 3.4 below.

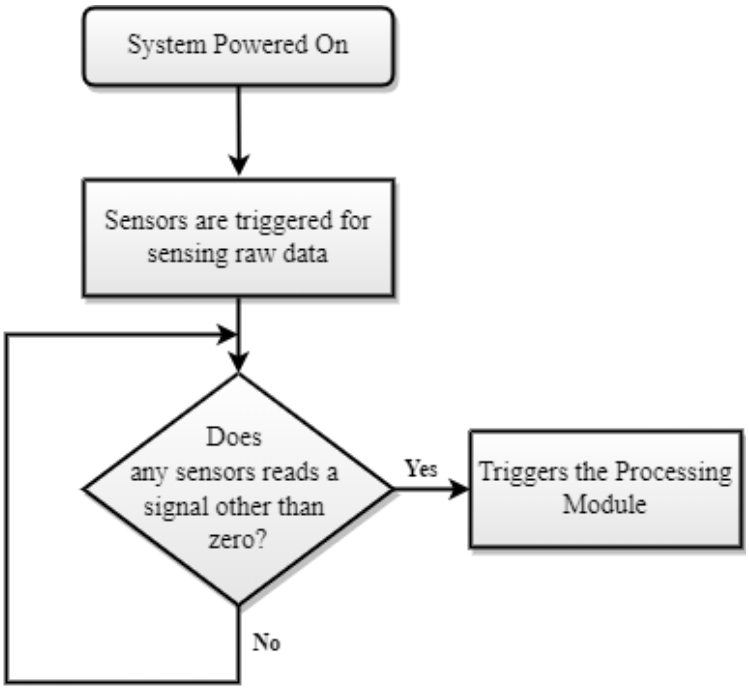

Figure 3.4 Sensing Module workflow

As soon as the system is powered on, it triggers the sensing module to sense the raw sensory data and once this data is available it is then send to the processing module where it gets converted into an interpreted physical data. This workflow continues till the system is powered on.

2. Processing Module

This module performs the processing of the received raw analog signals from the sensors by converting them into meaningful interpreted physical data. It is also responsible for actuating the actuators upon receiving the processed data from the other Robo Twin's arm processing module.

Another important task of this module is to actuate the servo motors of the fingers based on the pressure sensor data received from the sensing module. Upon receiving any nonzero signal from the pressure sensors located on the Robo Twin hand, it generates the control signals for the inward grasp of the user's hand. These control signals actuate the servo motors of each finger of

the Robo Twin's hand to grasp the subject's hand for a handshake. When the subject removes his contact from the located pressure sensors on the robo Twin's hand, it then generates the control signals for the outward grasp motion of the Robo Twin's fingers thereby releasing the user's hand and ending the handshake.

Simultaneously, while performing all the above-mentioned responsibilities, this processing module pushes the processed sensory data on the hardware serial ports of the micro controller for its transmission and real time recording.

3. Data collection Module

This part of the system's architecture is responsible for recording the sensory data while the Robo Twin is making a handshake with the user. This recorded data is later used for analysis purpose of the user's handshake characteristics over the period of handshake. This module gets in action as soon as the controller puts the processed sensory data into its default serial port (Serial Port 0). The microcontroller is connected to either the laptop or PC using a USB A to B converter cable as shown in the Figure 3.5 given below.

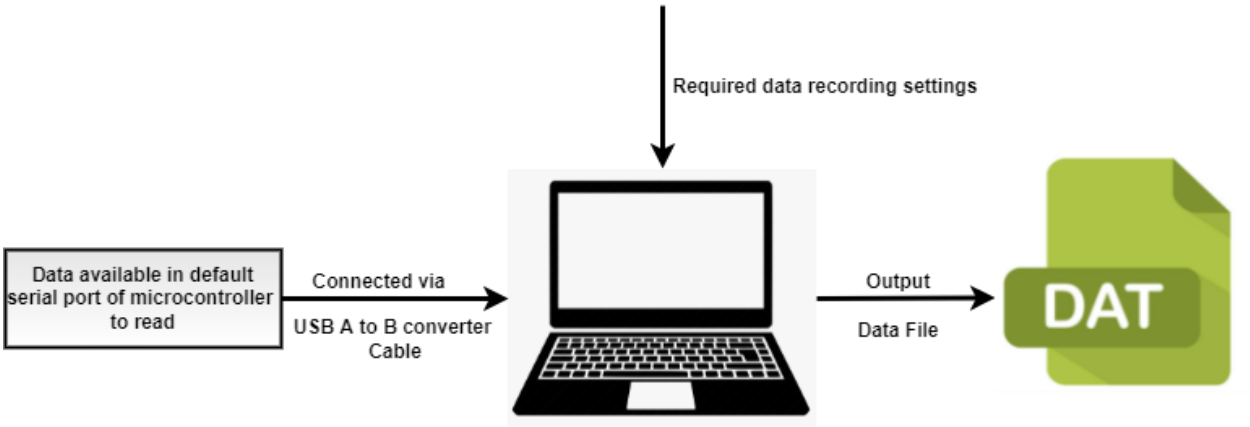

Figure 3.5 Data Collecting module workflow

Once the connection is successfully established, we can read and record the live data from pressure and temperature sensors by simply clicking on ***'Start Data'*** and ***'Record Data'*** respectively. When there is no data available in the serial port to be read and recorded, I.e., the Robo Twin has ended the handshake with the subject's hand, we can hit ***'Stop Data'***, to

terminate the connection and the data recording will be stopped. After the connection is terminated, it will generate a .xlsx file as an output which will have all the readings of temperature and pressure sensors along with their timestamps.

4. Data Transmitting and Receiving Module

This module is responsible for communication between the microcontrollers of the two Robo Twin arms for simultaneous and bidirectional transfer of sensory data. The transferred data is then received by the processing module of the other Robo Twin arm for actuating the corresponding vibrotactile pressure actuators to provide haptic feedback to the user. This simultaneous and bidirectional communication between the two microcontrollers is illustrated in the Figure 3.6 below.

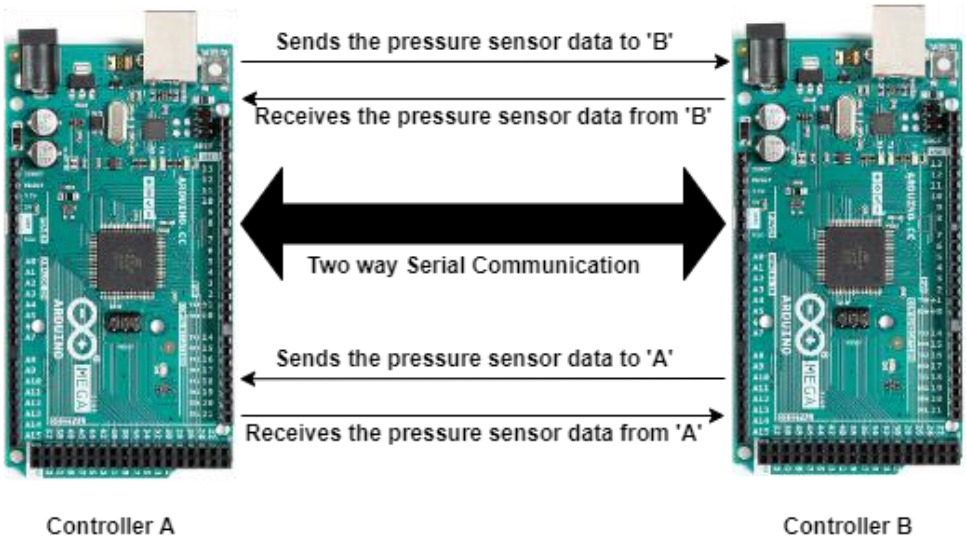

Figure 3.6 USART Communication between two Arduino Mega2560 microcontrollers

The communication between the two microcontrollers is achieved using USART Communication protocol. This is a serial type of communication technique which uses the hardware serial ports of both the controllers on either side. Since the processing module also uses the default serial port of both the microcontrollers for data collection, it is very important that the selected microcontroller have more than one hardware serial ports embedded within their architecture. Hence, the choice of Arduino Mega2560 as a microcontroller board in this project serves our purpose of interest.

3.4 Inmoov Robot's Arm Design

Inmoov [10], is the first Open-Source 3D printed life-size humanoid robot, designed by French designer Gael Langevin, costing around 2K USD. This robot has been used by several amateur researchers in the field of anthropomorphic robots because of its close to human like appearance, low cost, open-source nature, and feasibility to customize the design as per the needs of the application. The Inmoov design doesn't include any provision for the integration of specific sensors and actuators, this served as an advantage for us to combine the sensors and actuators as per our application needs within the given Inmoov design.

The Inmoov's arm design can be sub divided into three main parts namely, shoulder, bicep, forearm, and hand. The printing files and assembly instructions of all these parts are available on the Inmoov website.

Moreover, the Inmoov design is one of the best examples of an economical humanoid robot, whose parts can be easily 3D printed and assembled for a robust design. Because of its several advantages as highlighted, we decided to go with the Inmoov robots' arm design for our Robo Twins arm structure.

3.5 Summary

In this chapter, we have discussed the overall system's architecture and its different incorporated modules in detail and Inmoov based robotic arm design for the Robo Twin's Arm structure. Moreover, we have highlighted some major requirements of our proposed system and demonstrated how to achieve them.

4. Development of Robo Twin Arm

In this chapter we discuss the detailed Inmoov design of a Robo Twin's arm, placement of sensors and actuators, calibration of selected pressure and temperature sensors, and actuation of vibrotactile actuators of our proposed system in chapter 3.

4.1 Robo Twin's Arm Implementation

All the parts of the Robo Twin arm are 3D printed on a Ultimaker2+ printer with PVC as the printing material. The other printing settings including infill density, wall thickness, support, raft, beam, and nozzle size varies from part to part.

4.1.1 Robo Twin's Shoulder

For shoulder parts, an infill of 70%, wall thickness of 2.5mm, nozzle size of 6mm, and 'No' support settings are used to 3D print its parts. A total of 17 parts comprises of one right shoulder. For its actuation, hs-805bb heavy duty servo motor with a maximum torque up-to 10Kgs is housed inside the shoulder, giving it two degrees of freedom.

(a) Front view (b) Back view

Figure 4.1 Front and back view of Robo Twin's assembled right-hand shoulder

The front and back view of the assembled Robo Twin's right shoulder are shown in the Figure 4.1, demonstrating a 2 degree of freedom of the shoulder.

4.1.2 Robo Twin's Bicep

Similar to shoulder, for 3D printing the bicep parts, an infill of 70%, wall thickness of 2.5mm, nozzle size of 6mm and with 'No' support and raft printing settings are used. A total of 24 parts makes one right bicep. For its actuation, like in shoulder, hs-805bb heavy duty servo motors are enclosed within the bicep, providing it two degrees of freedom.

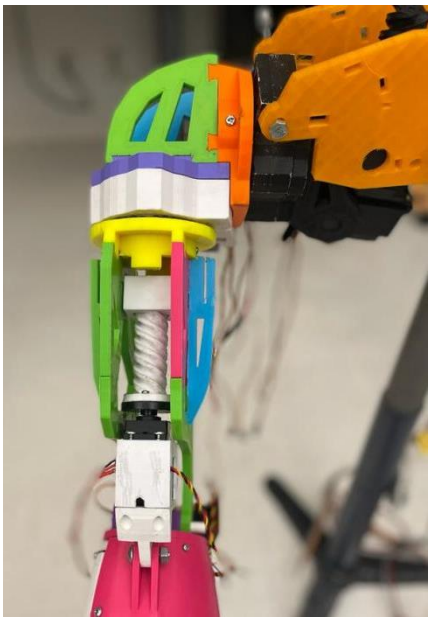

(b) Front view

(a) Side view

Figure 4.2 Front and side view of Robo Twin's assembled right-hand bicep

The front and side view of the assembled Robo Twin's right bicep are shown in Figure 4.2, demonstrating a 2 degree of freedom of the bicep.

4.1.3 Robo Twin's Forearm and Hand

For 3D printing both forearm and hand, an infill of 80%, wall thickness of 2mm, nozzle size of 6mm and with 'No' support and raft settings are used to print their parts. However, the gears are printed with the best quality possible with an infill of 100%, wall thickness of 3mm, nozzle size of 4mm, 'No' support and raft as the printing settings with Ultimaker2+ printer.

The fingers shown in Figure 4.3 below, are almost the same size as that of an adult male human but the forearm is made a little longer and wider to accommodate the standard sized servo motors for the actuation of fingers and wrist as shown in the Figure 4.4.

Figure 4.3 Printer and assembled fingers of Robo Twin with middle, index, ring, pinky and thumb from left are similar in size as that of an adult male

A highly under-actuated mechanism is used to control the motion of the Robo Twin fingers with the phalanxes of each finger i.e., the distal, middle, and proximal, controlled with only a single actuator. The actuator used for the motion of these phalanxes is MG996R servo motor, placed inside the forearm.

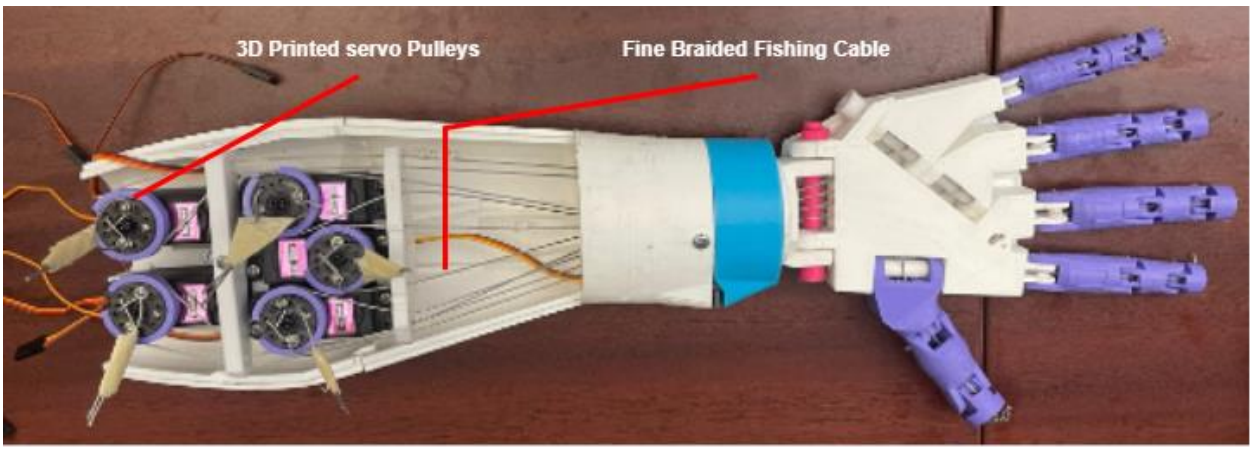

Figure 4.4 Forearm and hand of a robo twin with housed servo motors for fingers actuation via fine braided fishing line

The plastic servo horns that come with the servo motors are replaced by 3D printed servo pulleys through which a fine braided fishing line is passed as highlighted in the Figure 4.4. This braided fishing line makes it way to the fingertips after running through holes integrated within

the design, acting just like the tendons in the human body. At the servo end, the string is wound around the servo pulley and tied at one of its edges such that when the servo is operated, it rotates, and the string is pulled further to its edge thereby causing the fingertip to move in towards the palm. Therefore, the tension in the string causes the distal phalanx to bend inwards. As the tension keeps on increasing due to the torque provided by the servo motor, the middle phalanx followed by the proximal phalanx curls in too. Hence, the curling motion of the finger which constitute 3 DOF is achieved by making use of only one actuator. Fingers are returned to their normal resting position by just rotating the servos in the opposite direction by the same amount/angle.

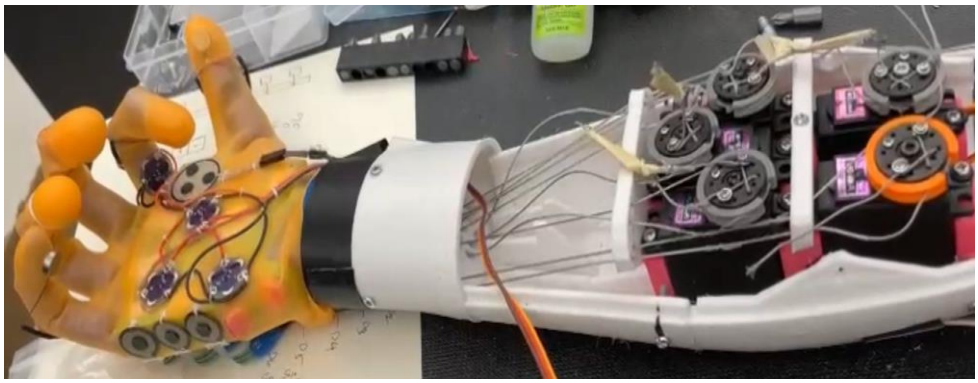

(a) Inwards motion of fingers achieved by rotating servos from 90° to 0°

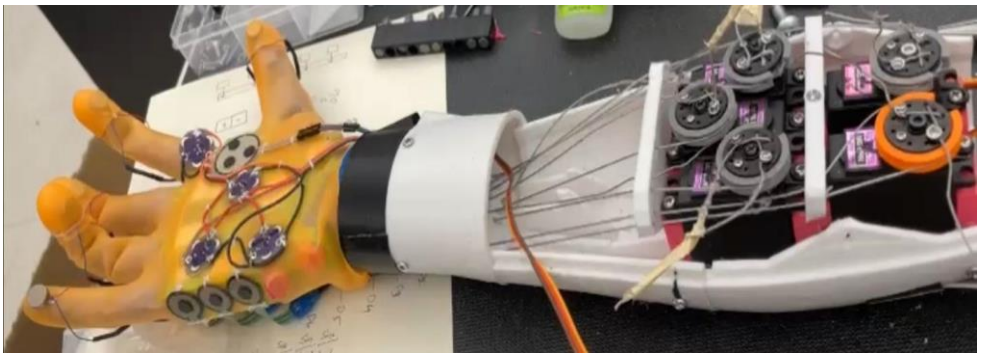

(b) Outwards motion of fingers achieved by rotating servos from 90° to 180°

Figure 4.5 Inwards and outwards motion of Robo Twin's finger

From programming point of view, all the servos' motors are set at 90°, this is the rest position at which there will is no slack in the tendons (fine braided fishing cables). Now to make the inwards motion of the finger, the servo motor is rotated to its extreme end I.e., to 0°. Similarly,

for outward motion of the finger the servo motor is rotated to its other extreme end I.e., to 180°. With this simple rotation of servo motor to 0° and 180°, the inward and outward motion of each finger is achieved. These conditions are illustrated in the Figure 4.5 above.

These servo motors each controlling all the three phalanxes of each finger were connected to the microcontroller and were successfully tested for their inwards and outwards motion using the technique described above.

4.2 Robo Twin's Pressure Sensors

Sensing pressure is one of the crucial tasks of our Robo Twin, designed and developed for the purpose of making a handshake with real human subjects. Our related work indicates that the Force Sensitive Resistor (FSR) is the most widely used technology in determining the contact forces in any application involving a robotic hand in the cited references. It is not only because of its low cost and ease of implementation but also for its relatively high sensitivity compared to capacitive tactile sensors and piezoelectric polymer films counterparts. Hence, the choice of FSR in our proposed Robo Twin system for the purpose of sensing contact pressure at different regions of hand contact while performing a handshake.

Sparks funs' 0.5" sensing dia and Teck scans' 1" sensing dia force resistive sensors are used in the implementation of pressure sensing in our Robo Twin's hand.

4.2.1 FSR's Voltage Divider Circuit

Although FSR is a nonlinear device which is highly sensitive to changes at low forces and much less sensitive to changes at high forces, a voltage divider with nonlinear transfer characteristics is employed to provide greater values of output at smaller values of sensor's resistance. Therefore, selection of the static resistor to pair up with the FSR is the trickiest part as we neither want to go over the highest resistance of FSR, nor we want to completely overshadow the lowest resistance of FSR. In most of the cases, a resistor with a value of 3.3kΩ is considered a good start as this value lies within the middle range of the FSR's resistive output.

However, it is observed and recommended that to increase the sensitivity of FSR at lower forces (usually few 100 grams) a higher value of static resistor must be used, and to have better sensitivity at higher forces (say around few kgs) a lower value of static resistor must be used. Since our goal here is to measure forces applied by different regions of the hand during a handshake by the real subject which mostly falls in the range of few 100 grams in case of a normal handshake and to have a better sensitivity in this low force range the choice of higher static resistance serves our purpose. Therefore, a resistor of 10KΩ is used as a static resistor to form a voltage divider circuit with the FSR.

4.2.2 FSR's Calibration

The selected sensors were then set up for their calibration against the known applied forces. The process of calibration is simplified with the help of Tinker Cad software as it allows the user to change the applied force on the FSR's sensing area from 0N to 10N and provides the output resistance of the FSR for each applied force.

The process of calibration includes the following steps:

1. Changing the known applied force on the FSR's sensing area.
2. Measuring the output of the FSR by means of Arduino code.
3. Studying the relationship between the applied force and FSR's output and determining a relationship between them.
4. Finally, running an independence test by placing a know mass on the FSR's sensing area to verify the established relationship between the studied parameters.

The schematic used for tabulating the FSR's resistive output for various applied forces is as shown in the Figure 4.6 below.

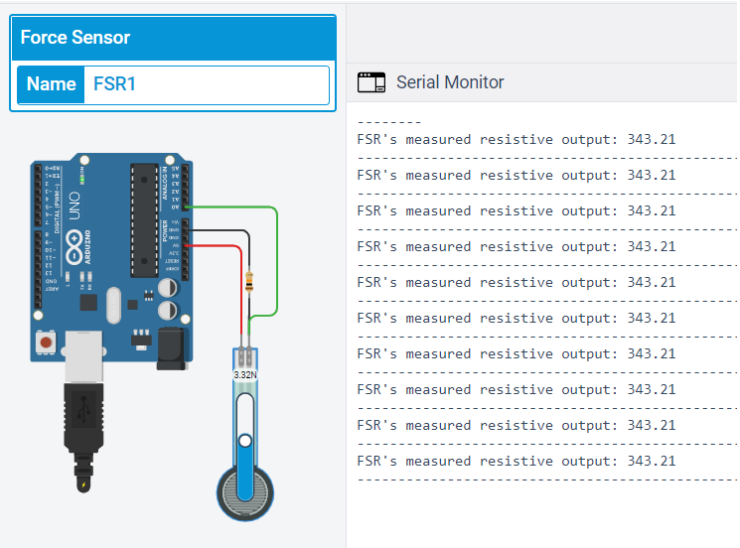

Figure. 4.6 Schematic diagram used for calibration of FSR sensor

Since we are interested in obtaining high sensitivity with FSR in its low force sensing range, the sensor is calibrated up to a maximum force value of 10N which is way more than the range that our application demands for normal handshake.

The graphs are plotted to visualize the graphical relationship between the Applied Force, and the measured resistive output of FSR, and calculated conductance. The graphical relationship between the applied force and measured resistive output of FSR is represented by the Figure 4.7 and the graphical relationship between the applied force and calculated conductance is represented by the Figure 4.8 respectively as shown below.

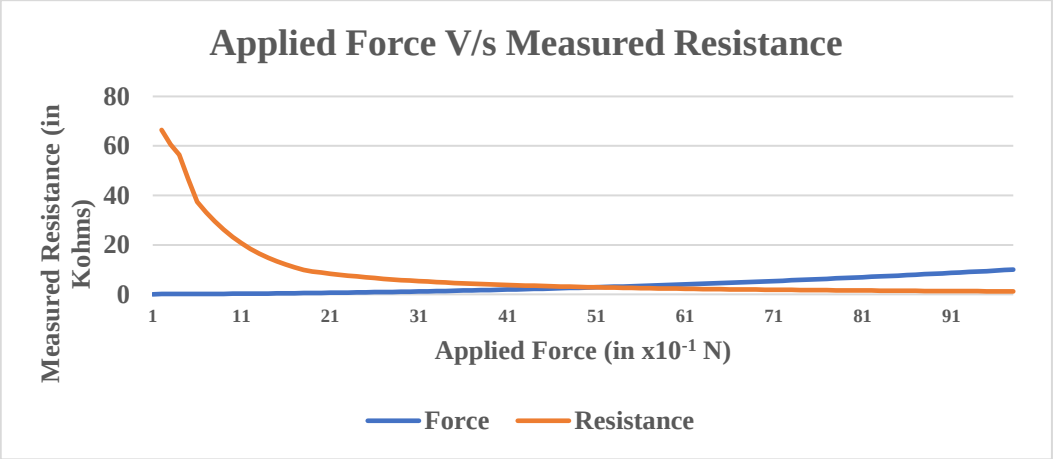

Figure. 4.7 Graphical relationship between applied force (N) and FSR's resistive output (KΩ)

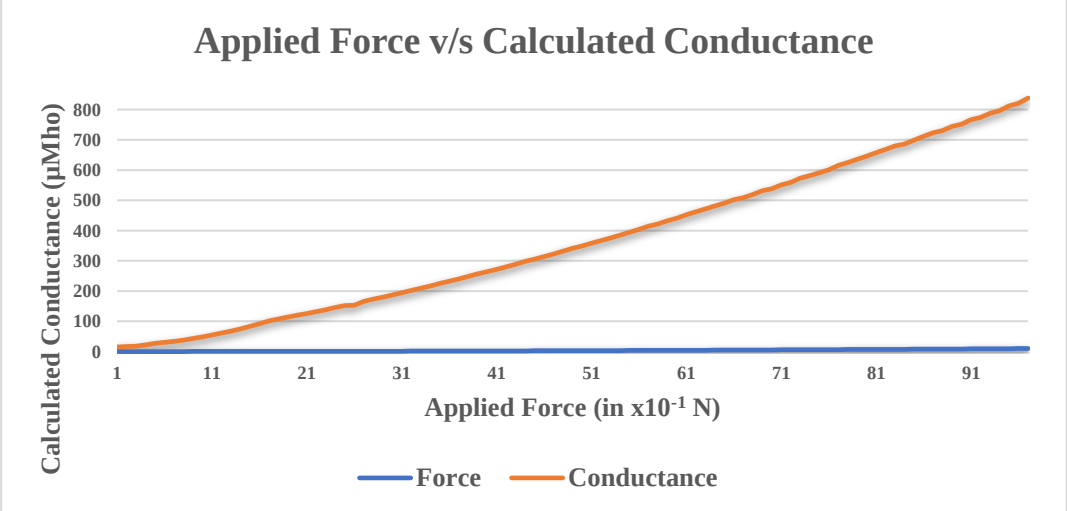

Figure. 4.8 Graphical relationship between applied force (N) and FSR's conductance (µMho)

It is clear that the FSR's conductance is a good measure of applied force as it varies almost linearly with the applied force than the FSR's resistive output which exhibits a nonlinear relationship with the applied force on FSR's sensing area.

To get a more detailed insight into the obtained data, the correlation coefficient, a measure of similarity between the two sets of data, is calculated. The calculated value of 'r', i.e., the correlation coefficient between the applied force and FSR's measured resistive output and calculated conductance is tabulated in Table 4.1.

Table 4.1 Correlation coefficient 'r' for different data sets

Data Set	**Correlation Coefficient 'r'**
Applied force and FSR's resistive output	-0.5179
Applied force and FSR's conductance	0.9906

Hence, the data set of applied force and conductance showed the highest similarity with 'r' being almost equal to 1. This indicates that the conductance parameter has a strong positive correlation with the applied force, which in turns also means that high conductance variable goes with high applied force variable and vice versa. Hence, to predict the applied force on the Force Resistive Sensor, the value of the calculated conductance is used rather than the direct measured resistive output.

Now, a simple linear regression which uses the least squares method to find the best relationship for a set of paired data, allowing to estimate the value of a dependent variable Y from a given independent variable X, is used to estimate the line of best fit. In our case, this regression equation can estimate the value of applied force (as a dependent variable Y) from the calculated conductance value (as an independent variable X) and is given by the equation $\hat{y} = mX + c$, where 'm' is the slope of the line and 'c' is the intercept (i.e., the value of Y when X = 0).

Running the linear regression test we get the equation as follows:

Applied Force (in N) = 0.01 * Conductance (in µMoh) - 0.83 …… *Equation (1)*

The line of regression represented by the equation 1 is illustrated by the Figure 4.9 shown below.

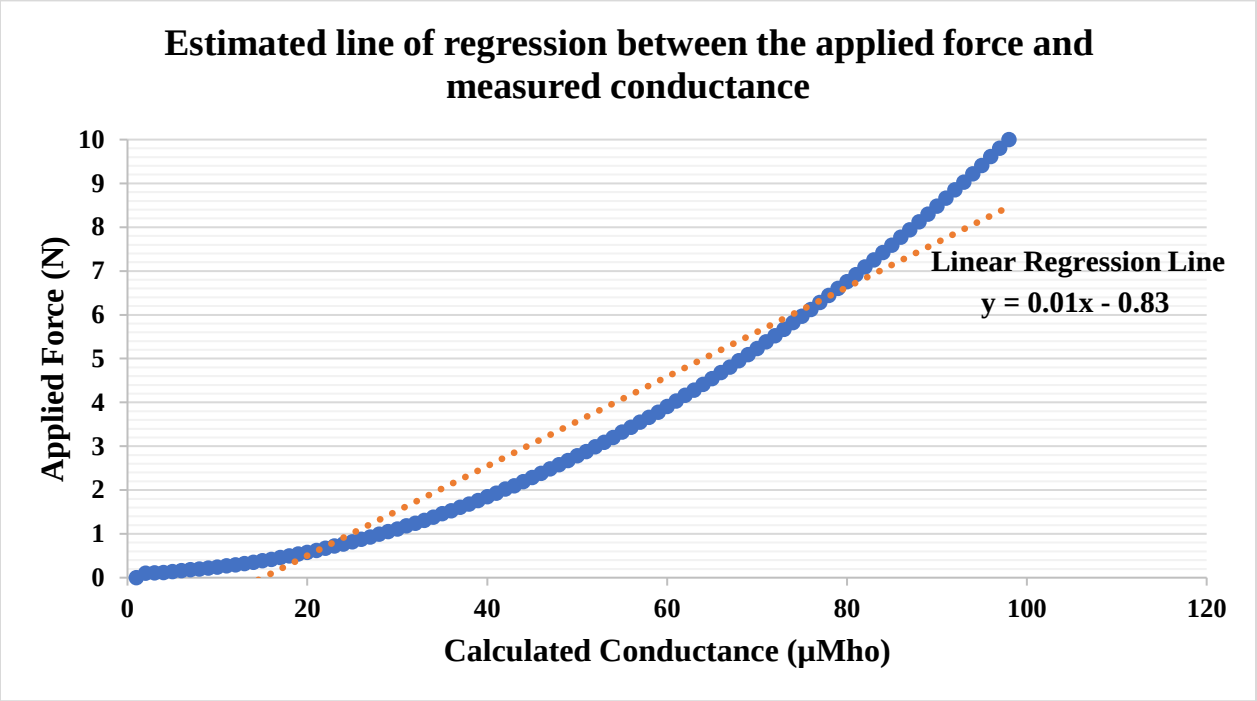

Figure. 4.9 Estimated line of regression between the applied force and measured conductance

As we can see from the above regression line graph, that the predicted force deviates from the actual values in the initial, final, and somewhat in the middle stages. To overcome this and to make our prediction more accurate we decided to divide the conductance into four different ranges I.e., from (0 to 120) µMho; (121 to 250) µMho; (251 to 600) µMho and (>600) µMho to find their separate regression lines.

Range 1: Conductance value in between (0 to 120) µMho

Running the linear regression test for this range of data set we get the regression equation as follows:

Applied Force (in N) = 0.0047 * Conductance (in µMoh) + 0.0347 …… *Equation (2)*

The line of regression represented by the equation 2 is illustrated by the Figure 4.10 shown below.

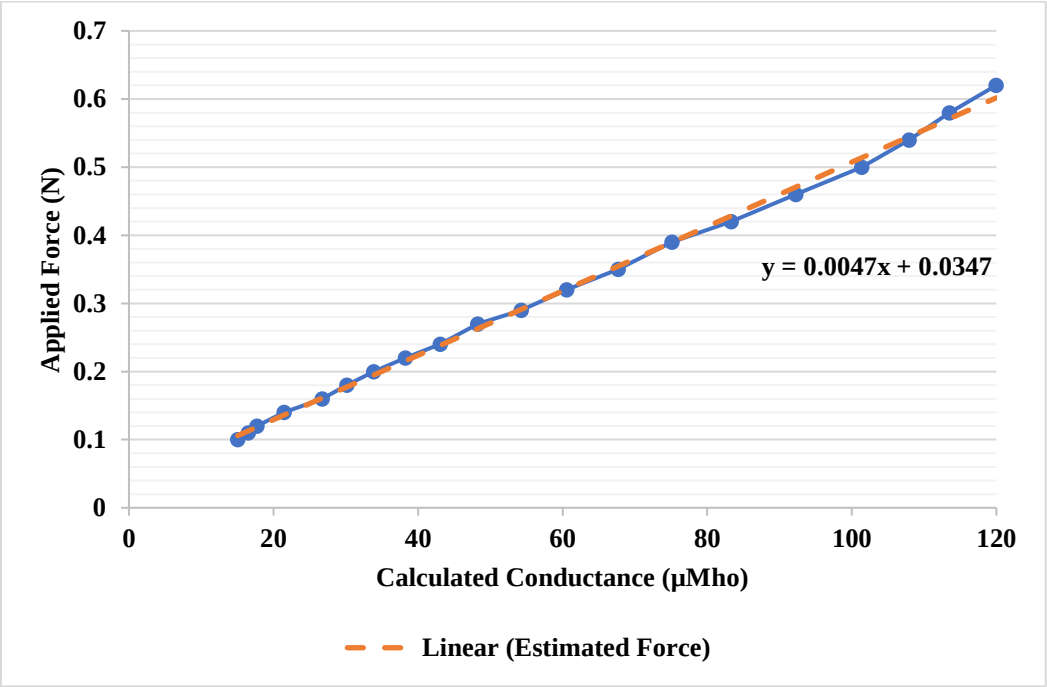

Figure 4.10 Estimated line of regression between the applied force and measured conductance in the range of (0 to 120) µMho

Range 2: Conductance value in between (121 to 250) µMho

Running the linear regression test for this range of data set we get the regression equation as follows:

Applied Force (in N) = 0.0088 * Conductance (in µMoh) - 0.4670 …… *Equation (3)*

The line of regression represented by the equation 3 is illustrated by the Figure 4.11 shown below.

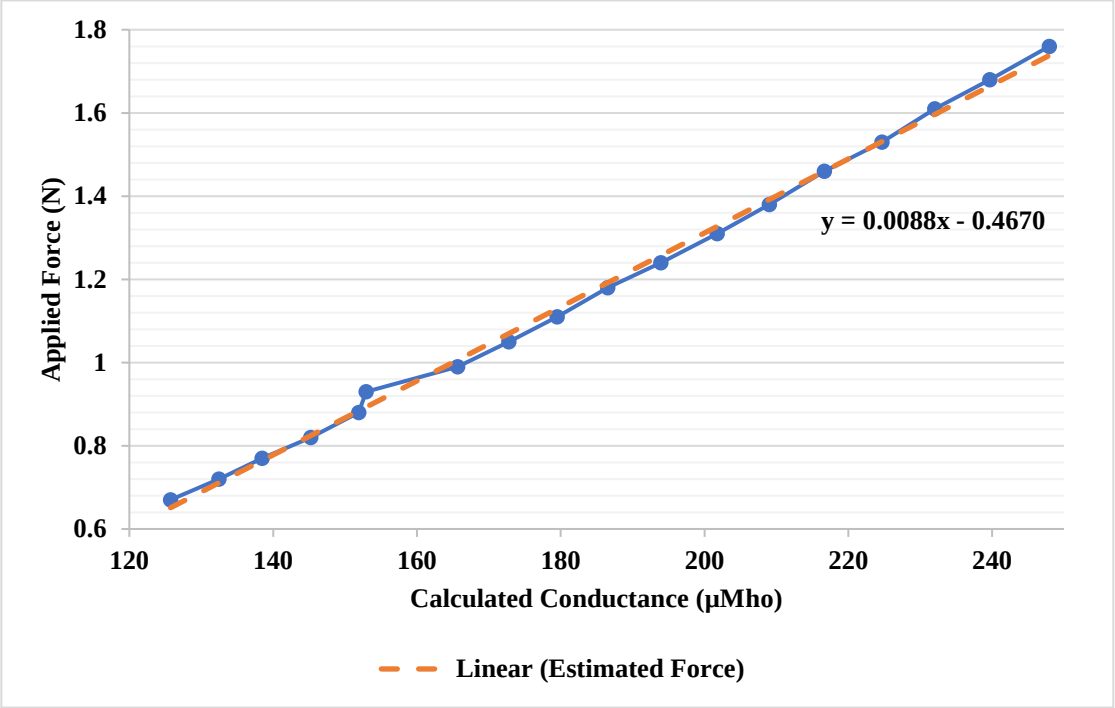

Figure 4.11 Estimated line of regression between the applied force and measured conductance in the range of (121 to 250) µMho

Range 3: Conductance value in between (251 to 600) µMho

Running the linear regression test for this range of data set we get the regression equation as follows:

Applied Force (in N) = 0.0127 * Conductance (in µMoh) – 1.5289 …… *Equation (4)*

The line of regression represented by the equation 4 is illustrated by the Figure 4.12 shown below.

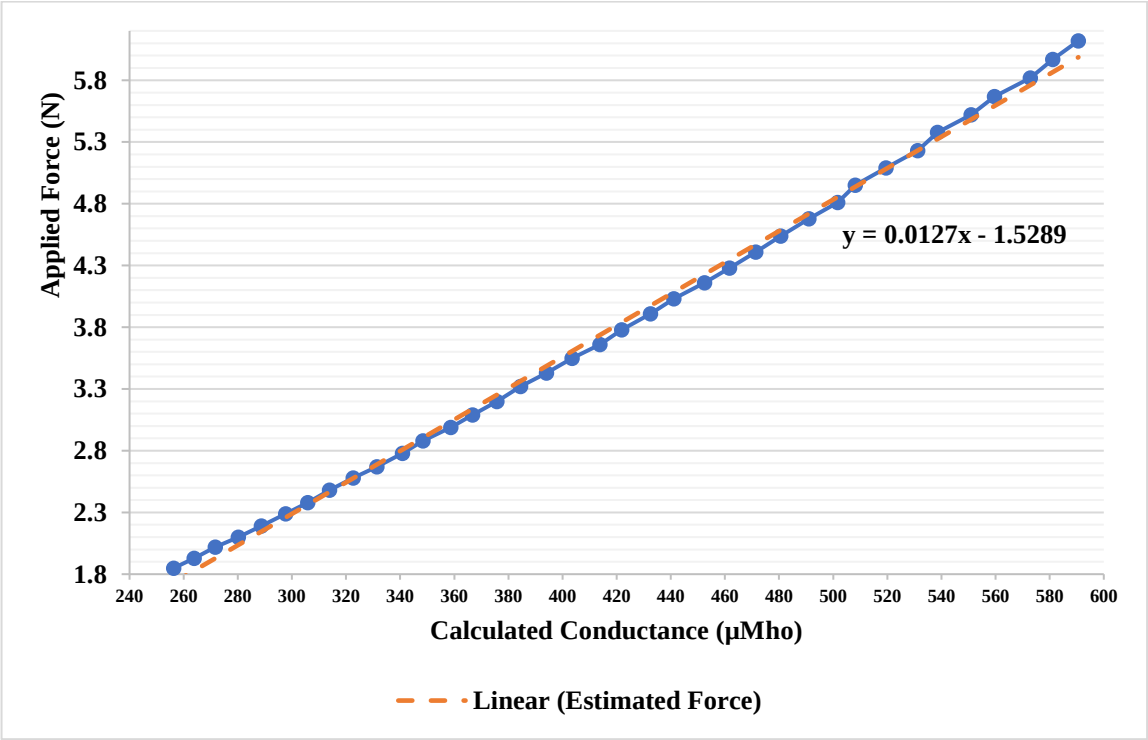

Figure 4.12 Estimated line of regression between the applied force and measured conductance in the range of (251 to 600) µMho

Range 4: Conductance value greater than 600 µMho

Running the linear regression test for this range of data set we get the regression equation as follows:

Applied Force (in N) = 0.0161 * Conductance (in µMoh) – 3.4949 …… *Equation (5)*

The line of regression represented by the equation 5 is illustrated by the Figure 4.13 shown below.

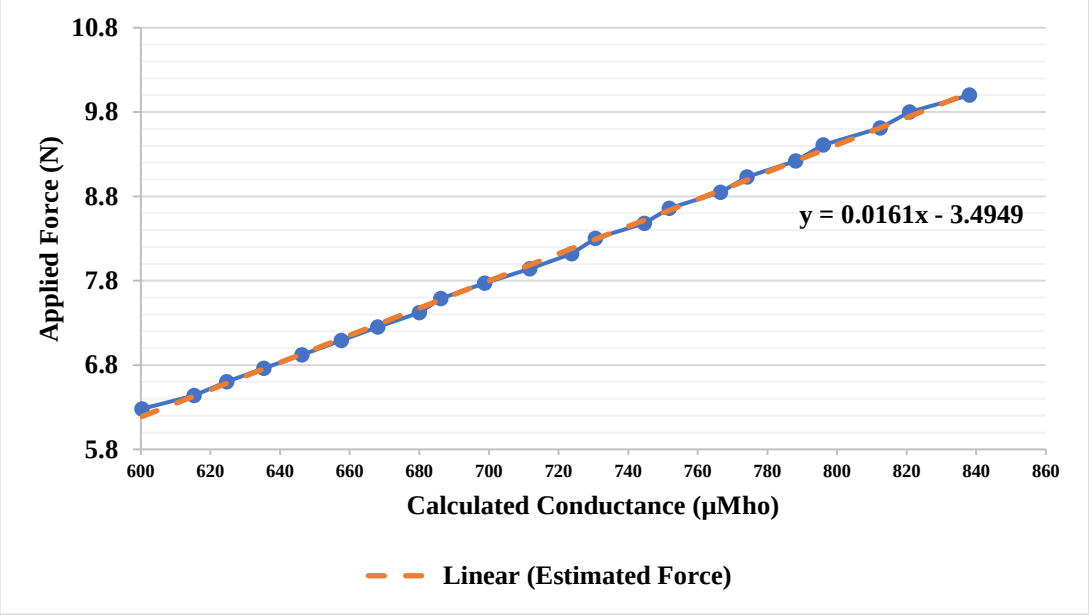

Figure 4.13 Estimated line of regression between the applied force and measured conductance greater than 600 µMho

Finally, to validate the calibration of the FSR sensor, a few independent tests are run by placing a know standard masses of 0 grams, 50 grams and 100 grams as shown in the Figure 4.14.

Figure. 4.14 Standard masses used to validate the calibration of FSR sensors

These standard masses are kept on the FSR's sensing area using the same schematic diagram as in Figure 4.14 to validate the calibration of the FSR sensors.

The results obtained from these independent tests for validating the calibration of FSR sensors are tabulated in the Table 4.2 below.

Table 4.2Calibration results of FSR sensor

Standard Weight (grams)	Equivalent Force (N)	Calibration Result (N)
0	0	0
50	0.49	0.50
100	0.98	0.96

The test results obtained are very close to the actual equivalent force values indicating a high accuracy of sensor calibration and validating the calibration process.

4.2.3 FSR Sensor Placement

As mentioned earlier in chapter 2, that there is a lack of research in analyzing the sensor placement on the robotic hands especially, in the application involving human-robot handshake. Due to this scarcity in the existing research, we came up with an elementary and a straightforward experiment to closely locate the pressure sensor points on the Robo Twin hand designed for performing a handshake.

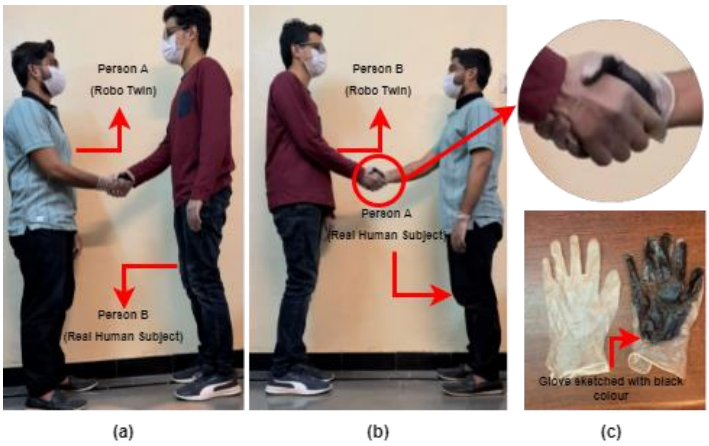

Figure 4.15 Handshake experiment to locate pressure sensing points of a human hand while performing a handshake

As a part of this experiment two real human male subjects, one having a bigger and wider hand size and taking the role of a Robo Twin (Person A) and the other with a comparatively smaller

and thinner hand and taking the role of a real human subject (Person B), were asked to perform a handshake with each other while wearing a white silicone hand glove as demonstrated in the Figure 4.15 (a). The glove of the person B was masked with black colour as shown in Figure 4.15(c), to get the imprints of his hand areas coming in contact with the person A's hand while making a handshake. The person B was asked to perform a strong and firm handshake with the person A to he feels the pressure on different regions of his hand coming in contact with the hand of person B and more importantly to get the imprints of the same regions on the glove of person A. After the handshake was complete, the glove of person A was analyzed for the areas of his hand that came in contact and experienced most of the pressure applied by person B.

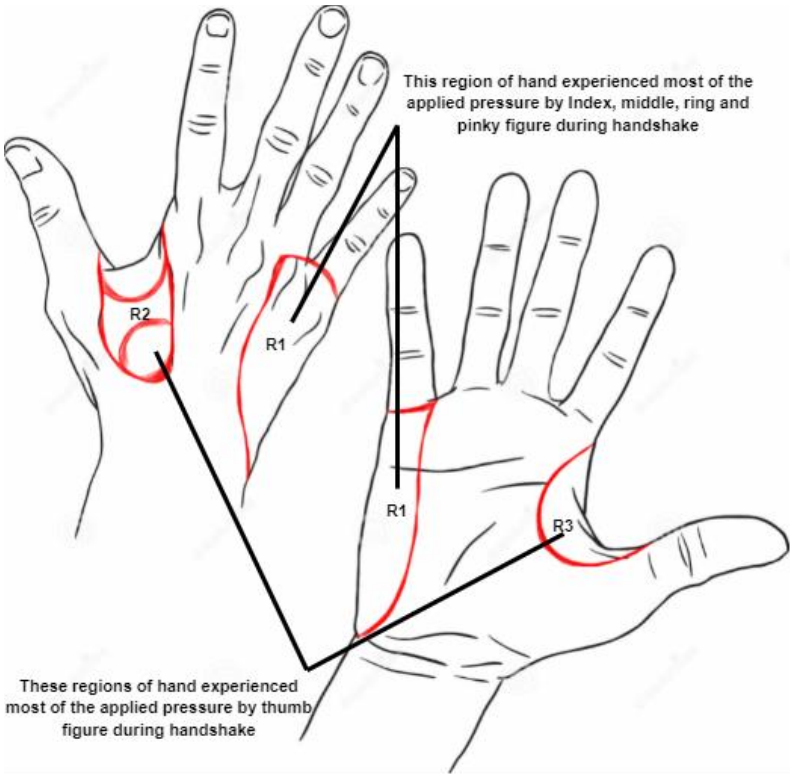

Figure 4.16 Mapped regions on the right hand for pressure sensor placement

The same procedure was repeated, but this time the roles of person A and B were swapped I.e., person B was now in the role of Robo Twin and the person A in the role of a real human subject represented in Figure 4.15 (b). Finally, the imprints obtained on the glove of persons imitating as a Robo Twin were observed and the overlapping areas from both the experiments were mapped on a right hand as illustrated in the Figure 4.16.

The regions highlighted by the red were found to be most in contact with the other hand during a handshake. The region R1 is the area where the pressure applied by the index, middle, ring and pinky finger of the real subject can be sensed and similarly regions R2 and R3 are the areas where the pressure applied by the real subject's thumb finger can be sensed. These areas of real subject's hand applying pressure on the person's hand imitating as a Robo Twin, while performing a handshake are represented in the Figure 4.17.

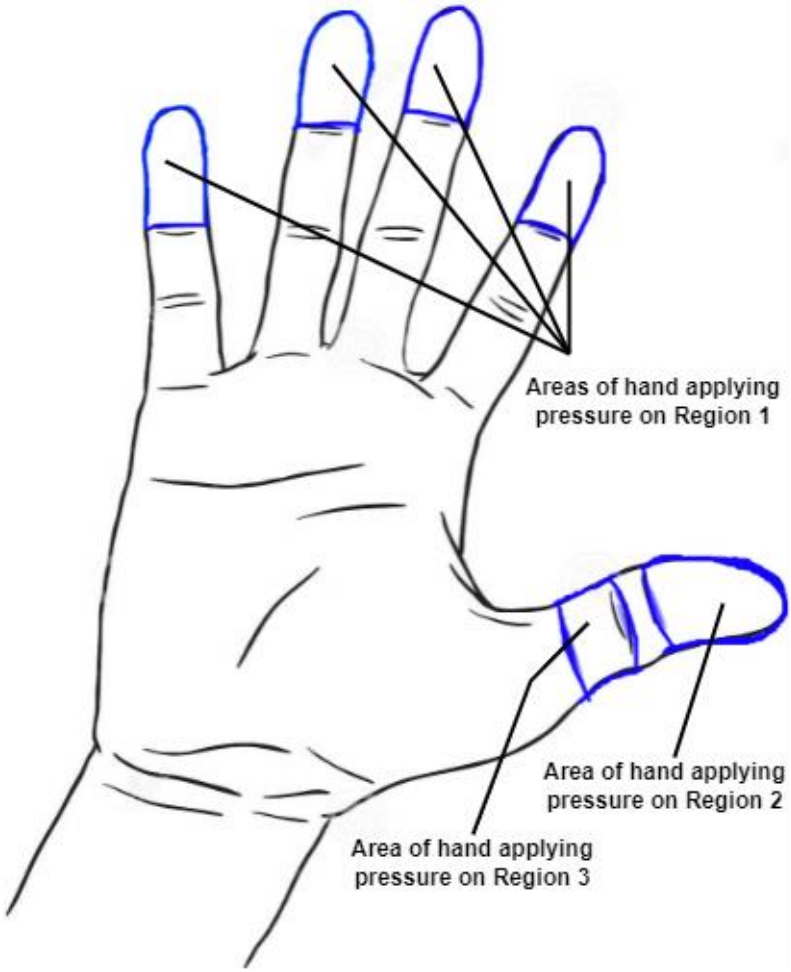

Figure. 4.17 Regions of the hand applying most of the pressure during the handshake

Finally, we have the location of placing pressure sensors on the Robo Twin hand for sensing of force applied by the real subject's hand, while performing a handshake, based on our above analysis. These areas were observed on the actual Robo Twin's hand to estimate the number of pressure sensors required to effectively cover these pressure sensing areas as highlighted in Figure 4.17.

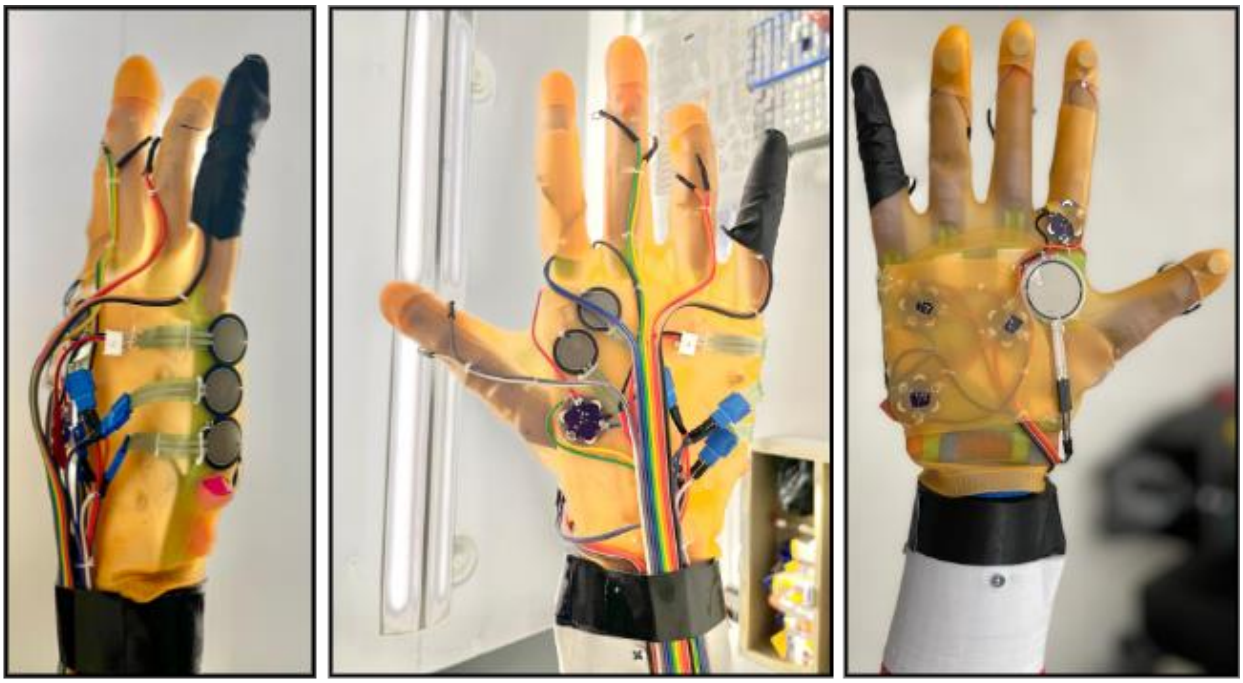

Placement of 3 Sparksfuns' 0.5" sensing dia FSR's in Region 1

Placement of 2 Sparksfuns' 0.5" sensing dia FSR's in Region 2

Placement of 1 Teckscans' 1" sensing dia FSR's in Region 3

Fig 4.18. Placement of six pressure sensors on an actual Robo Twin Hand

A total of six pressure sensors, 5 Sparks funs' 0.5" sensing dia and 1 Teck scans' 1" sensing dia, were used to cover the pressure sensing areas of the Robo Twin's hand as shown in Figure 4.18 above.

4.3 Robo Twin's Temperature Sensors

Sensing temperature of real twin's hand while performing a handshake is another critical task of our Robo Twin hand design. From the literature survey presented in chapter 2 of this thesis, the most widely used temperature technology for measurement of temperature of objects in contact with the robotic hand is based on the use of Thermistor as a temperature sensor. Therefore, we decided to use Lilypad's MCP9700, a small thermistor type temperature sensor for detecting temperature changes because it not only provides ease of calibration and implementation but also it can be sewn into any fabric as it is developed for the purpose of wearable e-textile technology. Moreover, these sensors are even washable, so there is no fear of damage to sensor due to sweat, if any, coming in contact with the sensor during the handshake.

The later section discusses, the calibration and placement of Lilypad's MCP9700 temperature sensor and schematic diagram used for the implementation of temperature sensing aspect of our Robo Twin.

4.3.1 Lilypad's MCP9700 Calibration

From the information made available through the data sheet of this particular temperature sensor, the calibration process is made much easier. This sensor outputs specific voltage values at set temperatures, I.e., 10mV for every degree rise in temperature with 0.5V level set for 0°C. The analog signal read by the microcontroller at the signal line of the temperature sensor is converted to digital signal using analog to digital conversion, to establish the temperature of the object in contact with the sensor as the voltage output by the sensor is linearly proportional to the Celsius temperature.

Therefor, once we know the output voltage of the sensor, we can calculate the temperature of the object in contact with the temperature sensor using the following equation

Temperature in Celsius (°C) = (Sensors output voltage - 0.5) * 100 …… *Equation (6)*

4.3.2 Temperature Sensor Placement

With no existing research in this area of temperature sensor placement on the robotic hand for sensing the temperature of real human subject's hand while making a handshake, we decided to refer to the findings of the experiment performed in section 4.2.2 of this chapter, where we asked two real human subjects to perform a handshake while wearing white silicone gloves with one of them masked with black colour to get the imprints of the areas in contact with the other hand during a handshake.

In order to effectively locate the temperature sensor points, we carefully analyzed the regions of hand coming in contact with each other during handshake and the parts of the hand responsible for its sensing. The findings of this experimental observations are illustrated in the Figure 4.19.

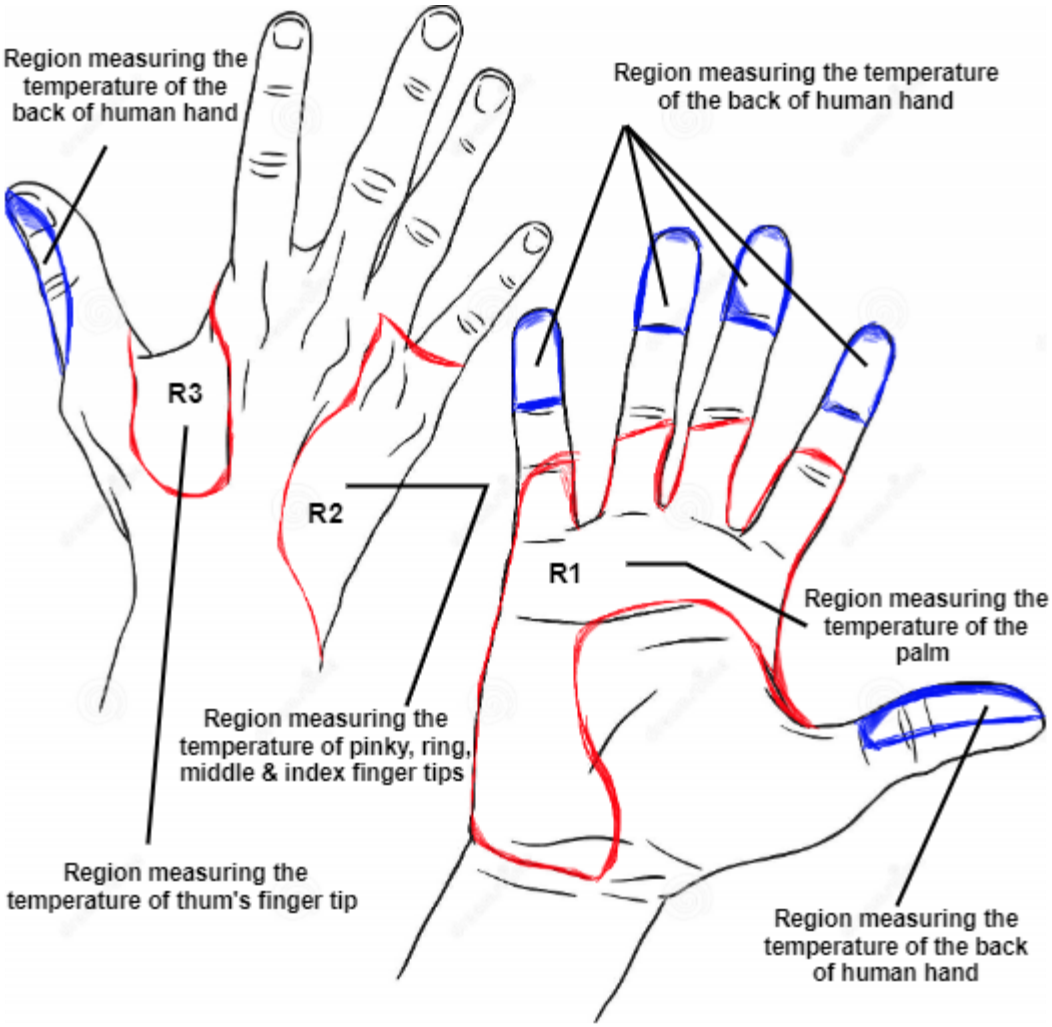

Figure. 4.19 Different regions of hand measuring the inside and outside temperature of the hand

In the Figure 4.19, the regions R1, R2 and R3 of hand highlighted by red colour senses the temperature of the real subject's hand while the area highlighted by blue colour senses the temperature of the backside of real subject's hand when performing a handshake.

For the actual placement of the temperature sensor on the Robo Twin hand we only focused on the sensing of temperature of the real subject's front hand and not the backside of hand. As far as region R2 and R3 are concerned, which are sensing the temperature of fingertips, we decided only to implement the region R3, as the temperature of all fingertips are almost the same at any given point of time. This will avoid the redundancy in the sensed temperature data.

This implementation of the temperature sensors on the actual Rob Twin hand is demonstrated in the Figure 4.20.

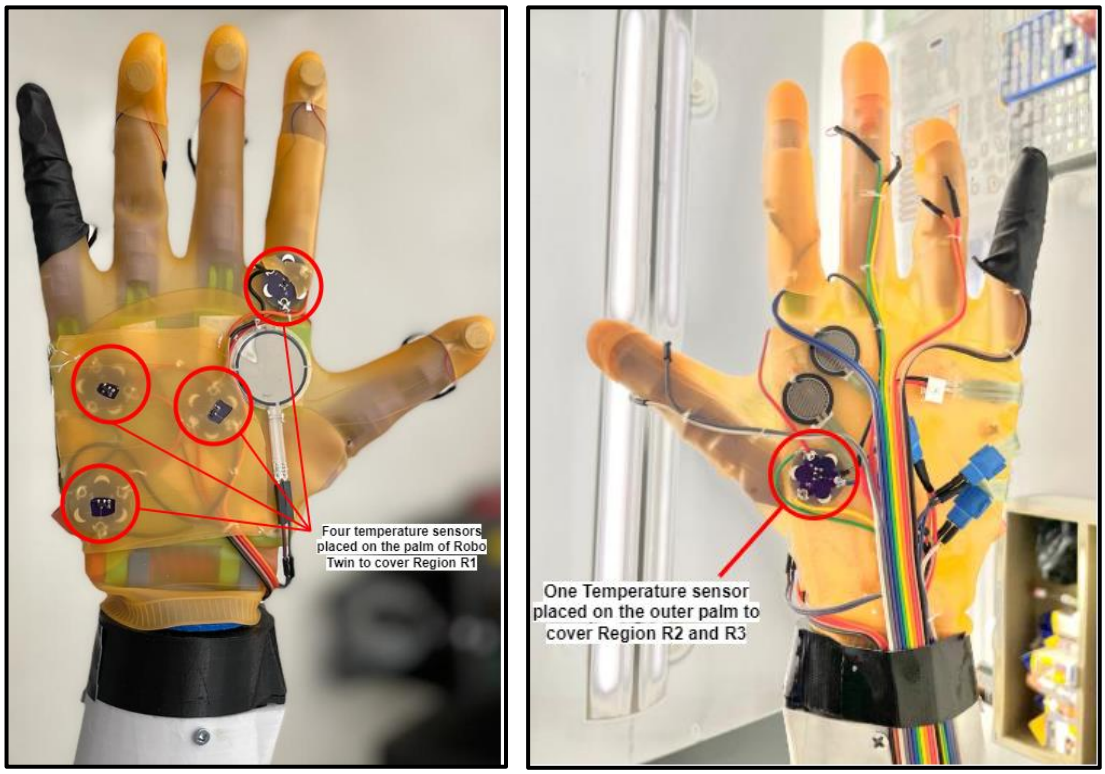

Figure. 4.20 The actual placement of temperature sensors to cover sensing regions R1, R2 and R3

A small cut in the silicone glove is made just over the temperature sensor to prevent the effect of silicone from interfering with the actual temperature reading of the object in contact with the temperature sensor.

4.4 Robo Twin's Vibrotactile Actuators

To provide force feedback on either side of the Robo Twin for the real subjects to experience and feel the amount of equivalent pressure being applied by each of them on either side, we decided to use vibrotactile actuators, specifically, Eccentric Rotating Mass (ERM) types of vibration motors rated 13000 RPM and operating at 5V DC.

To make the force feedback more effective and closely imitating the movements of the regions of real subject's, hand that are applying pressure on the Robo Twin's hand, a Spark sun's DRV2605L haptic motor driver is used to operate these vibrotactile ERM motors. Although, this

haptic motor driver provides various inbuilt functionalities, we are more concerned on the PWM input (0% to 100%) Duty-Cycle Control Range function accommodated by this haptic motor driver to control the frequency of vibrations of these motors based on the received input PWM signal from the microcontroller.

The later section discusses the calibration, placement, and implementation of these vibration ERM motors for providing a real force feedback.

4.4.1 Vibration ERM Motor Calibration

The received pressure sensor readings from the FSR sensors are provided as input to the vibration ERM motors. The analog output value from each corresponding FSR sensor is mapped using the inbuilt map () provided by the Arduino IDE. This function remaps a number from one range to another, I.e., it maps a value of ‘fromLow’ to ‘toLow’ and ‘fromHigh’ to ‘toHigh’. Therefore, the output analog value from the corresponding sensor is remapped and the resulting value is given as a PWM input signal to the haptic motor driver DRV2605L, which in turns operates the vibration ERM motors to give the equivalent gradual effect of the applied pressure sensed by the FSR sensors by adjusting its vibration frequency.

4.4.2 Vibration ERM Motor Placement

For its placement, we refer to the Figure 4.17 which illustrates the regions of hand applying the most pressure on the Robo Twin hand while making a handshake, hence, for the Robo Twin hand in the actuation phase, these areas of its hand must apply the pressure on the real subject’s hand I.e., to provide the equivalent gradual force being sensed by the corresponding region’s FSR sensors. However, due to our design constrains we are not able to implement the force feedback by the region 3 in the Figure 4.17.

The mapped regions on the right hand for the placement of vibrotactile actuators are represented by the Figure 4.21 given below.

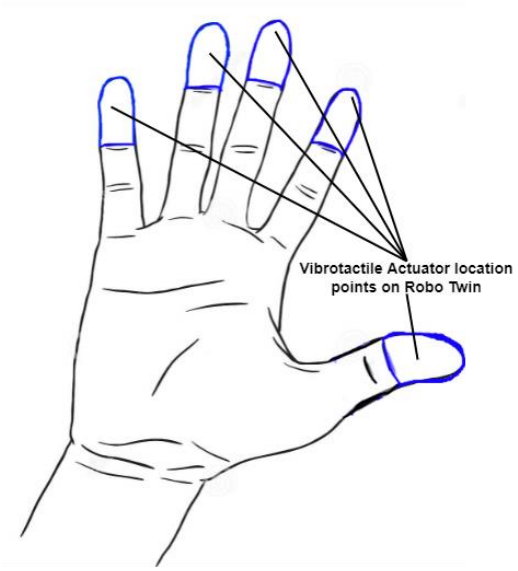

Figure. 4.21 Mapped regions on the right hand for the placement of Vibrotactile actuators

And the actual placement of these actuators on the Robo Twin hand are shown in the Figure 4.22 below.

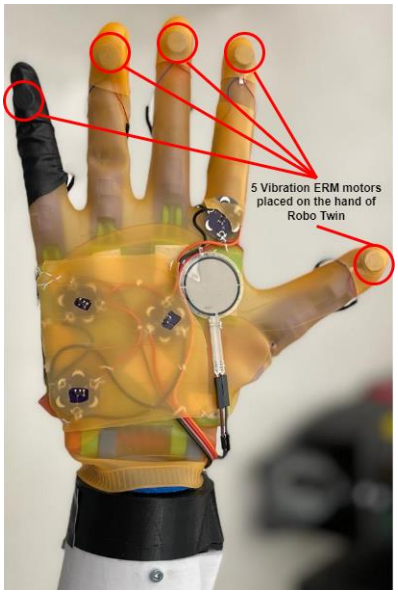

Figure. 4.22 Placement of Vibration ERM Motors on actual Robo Twin hand for force feedback

Each ERM motor requires one DRV2605L Haptic Motor Driver, as this motor driver can control only one vibration motor. The individual connection of each Vibration ERM motor with the

haptic motor driver DRV2605L and the microcontroller Arduino Mega2560 can be seen in the Figure 4.23 below.

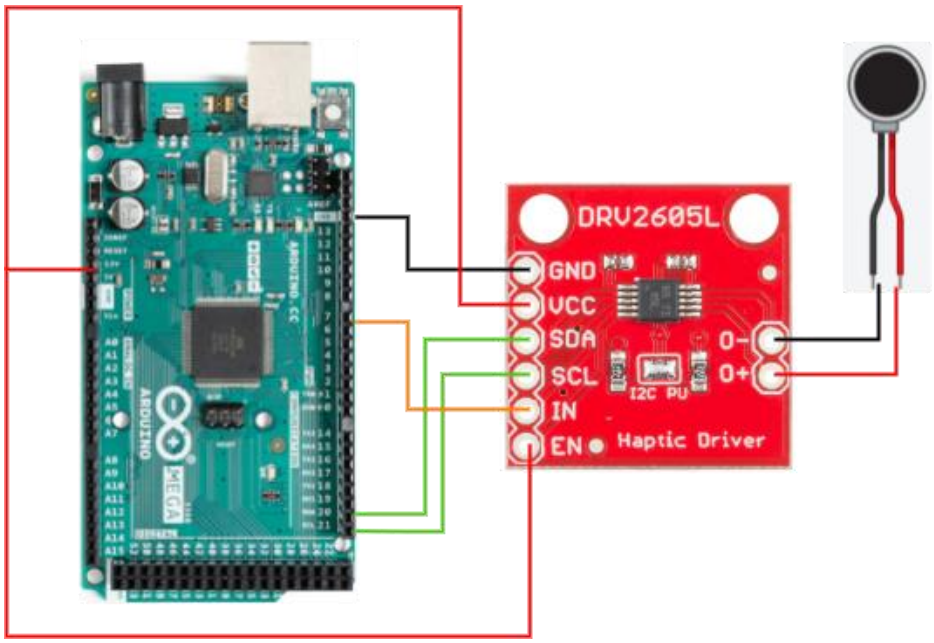

Figure. 4.23 Circuit connections of DRV2605L and Vibration ERM Motor with Arduino Mega2560

Therefore, a circuit board, containing five such DRV605L motor drivers, is made to incorporate the five ERM motors placed on each hand of the Robo Twin.

5. Performance Evaluation

In this chapter we present both the qualitative and quantitative analysis of our proposed Robo Twin system based on the human-robot interaction while making a handshake. The two designed Robo Twin right arms were evaluated by considering both male and female participants with a different age range. The later sections of this chapter, describes the experimental setup and procedure, its test objectives and finally the results of our analysis.

5.1 Experimental Setup

To evaluate the performance of our proposed Robo Twin concept, the designed system with two right Robo Twin arms were setup in Bio Informatics Lab at the University of Ottawa.

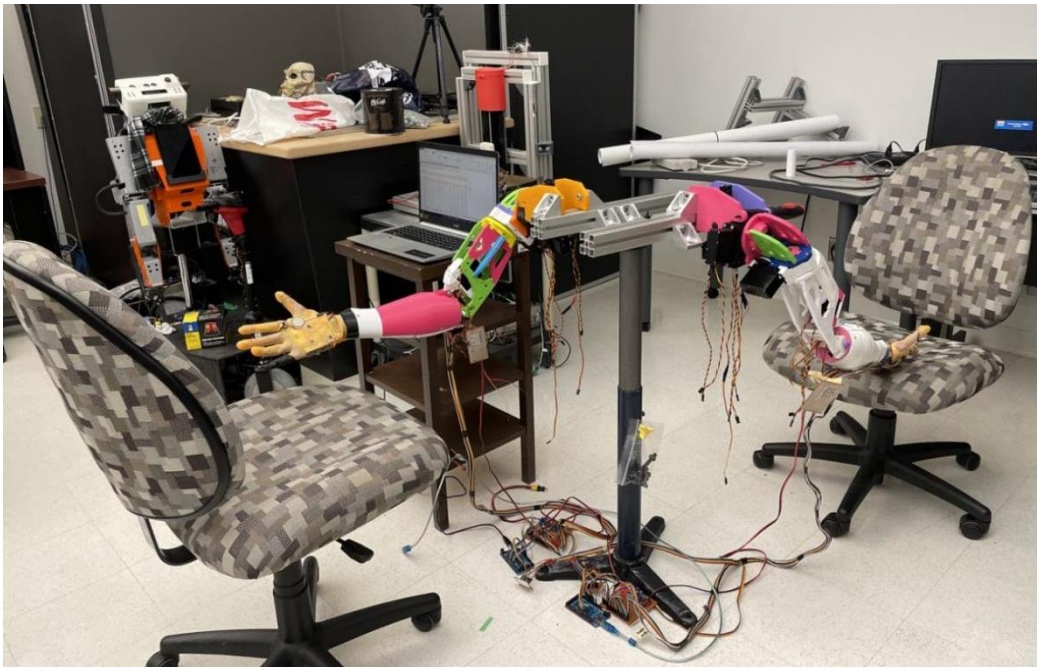

Figure 5.1 Robo Twin handshake experiment setup

The setup includes two right Robo Twin arms mounted on a 3ft pole on either side as shown in the Figure 5.1. Each arm is connected to a laptop via a USB A to B converter cable to record the

experimental data from each arm. Also, there is a chair kept in front of the arms for the participants to sit and comfortably make a handshake with the Robo Twin hand.

5.2 Experimental Procedure

A total of 18 participants consisting of 8 male and 10 female subjects with a different age range took part in both the quantitative and qualitative analysis of handshake experience with Robo Twin. For each experiment, two participants are required on each side of the system. Prior to the experiment, the participants were explained on how to interact with the Robo Twin arm and were given detailed step by step flow of the experiment, as mentioned below:

1. The two participating individuals were first asked to shake a hand with each other as they would normally do, and then they were asked to make a strong and firm handshake. This step is necessary to familiarize the participants with their pressure points and feel of the force feedback that they are receiving from the other person in both cases to differentiate between the normal and a stronger handshake.
2. The participants then take their respective positions, sitting on chair, in front of each Robo Twin arm.
3. The participants will move their hand to grasp the hand of the Robo Twin for the purpose of making a handshake.
4. The Robo Twin will in return grasp the hand of the participant as soon as the participant makes a contact with any of the pressure sensors placed on the Robo Twin hand, completing the handshake initiated.
5. During the handshake, participants are asked to go gradually from a normal to a firmer and a stronger handshake.
6. After the pressure sensor data is transferred bidirectionally between the two Robo Twin arms by means of serial communication between the microcontrollers of the system, the vibrotactile actuators will be actuated and each participant will now be able to simultaneously feel the equivalent force being applied by the other participant on the other side of the system.
7. At this point, when the participants are moving from a normal to a firmer and a stronger handshake, they are asked to verbally verify the same with the other participant whether they can feel the difference of applied pressure by them. Thereby differentiating

a normal from a firmer and a stronger handshake. This also justifies the proper force feedback being provided by the system on either side based on the sensed pressure data.

8. Once the participant's contact with the pressure sensors presents on the Robo Twin hand ends, this indicates the Robo Twin that the participant is willing to end the handshake. Therefore, the Robo Twin will release the participant's hand making an end to human-robot handshake.

9. Finally, recollecting their experience of real handshake performed with each other prior to the experiment with the Robo Twin arm, each participant is asked to complete a short survey to provide their overall feedback on their interaction with the Robo Twin arm and the overall system.

Meanwhile, during the phase of the experiment, the pressure and temperature sensor data is collected for further quantitative analysis of human-robot handshake.

Later the participants were invited to take two personality assessments. The first one to assess the BIG FIVE traits of one's personality namely Extraversion, Emotionality, Conscientiousness, Agreeableness, and Openness [52], and the second one is the positive and negative affect scale (PANAS) test [53] to assess how they generally feel.

5.3 Test Objectives

The overall haptics and human-robot experience is highly dependent on one's personal preferences. These are more apparent in a situation like a handshake, as every other person has their own personality and mental physiology. Through our designed Robo Twin hand and this experiment we aim at understanding the participants overall handshake characteristics and their experience with the Robo Twin arm and the overall system in general. Therefore, the test objectives can be listed as follows:

1. To assess the adaptability of our Robo Twin concept by the users.

2. To evaluate the overall human-robot interaction as perceived by the participants while making a handshake with the Robo Twin arm.

3. To study the handshake characteristics of the participants like their grasp, sensing their hand temperature and pressure being applied by various regions of the hand during a

handshake and to find a correlation between these handshaking characteristics and the gender and personality traits of the participants.

5.4 Experimental Results

These experimental findings are classified into qualitative and quantitative analysis, where the qualitative analysis reflects the overall haptics and human-robot experience as perceived by the participants and quantitative analysis aims to provide an insight into physical handshake characteristics like the duration of handshake, the temperature of the participant's hand, and the force being applied by various regions, and the correlation between these handshaking characteristics and the gender and the personality traits of the participants.

5.4.1 Qualitative Analysis

The qualitative analysis of our Robo Twin system is achieved through a post experiment questionnaire with a total of 12 questions based on different experiences that the participants had during their period of handshake with the Robo Twin arm. Moreover, these questions use Likert scale, where the participants are asked to rate their experience on a scale of '1' to '5', with '1' indicating the lowest rating and '5' indicating the highest rating, rather than just a 'Yes' or 'No'.

It was interesting to note that, 61.1% of participants rated that they are likely to use our Robo Twin system to connect to their loved ones remotely and perform a handshake and 27.8% of them had a neutral perspective about our system.

Table 5.1 below represents the twelve post experiment questions and their average results.

Table 5.1 Average results for the post experiment questionnaire

Question #	Questions	Average
1.	How would you rate the initiation of handshake by the Robo-Twin?	3.7
2.	In comparison to a human-hand grasp, how similar did you feel the hand grasp of Robo-Twin was?	3.2
3.	How would you rate the force feedback, that you received from the Robo-Twin?	4.4
4.	How different was your experience during a handshake with Robo-Twin: from a weak to a stronger handshake by the same participant on the other side?	3.7
5.	How different was your experience during a handshake with Robo-Twin: with two different participants on the other side?	3
6.	In comparison to a human-human handshake, how would you rate your duration of handshake with Robo-Twin?	3.1
7.	To what extent do you think the system responded precisely to your handshake/hand movements?	3.9
8.	To what extent do you think the Handshake with the Robo-Twin was useful and natural?	3.4
9.	How would you rate your overall haptics experience with Robo-Twin?	4.2
10.	How would you rate the overall handshake experience with the Robo-Twin?	4.1
11.	To what extent do you find the Robo-Twin intuitive?	4.3
12.	Given a situation, where you and your loved ones are physically distanced but remotely connected, how likely are you to adopt our concept of Robo-Twin to have a handshake with your loved ones?	3.8

The Figure 5.2 summarizes the results of the post experiment questionnaire based on likert scale on the range of 1 to 5.

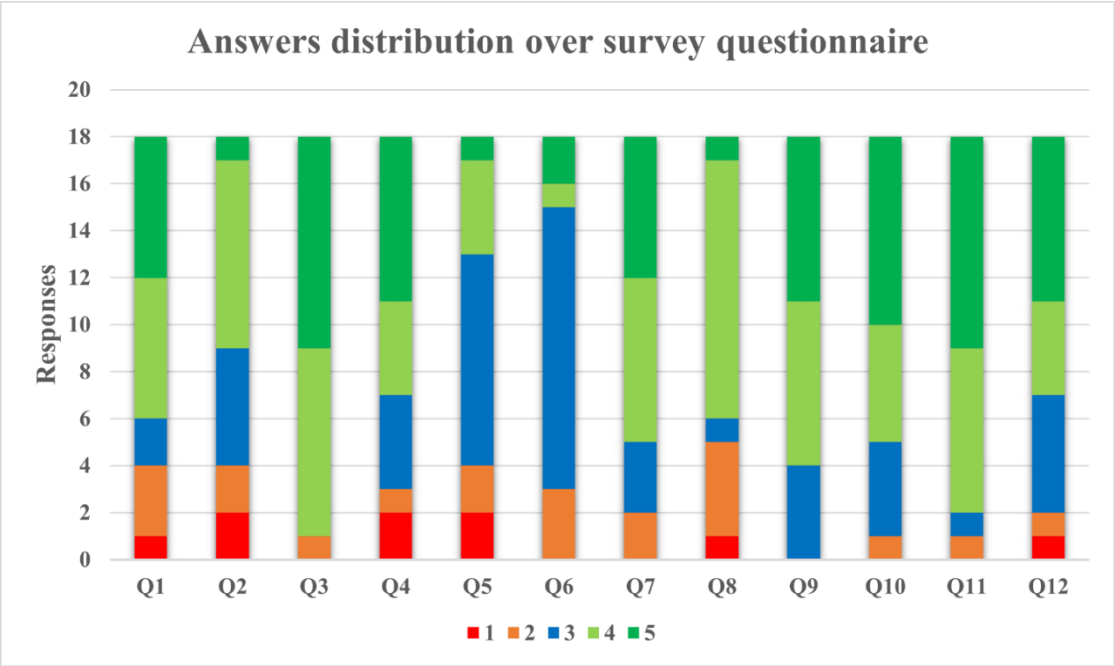

Figure 5.2 Distribution of responses to the survey questionnaire

After the post experiment questionnaire, we also had an open-ended question where we asked the participants to share their overall experience in their own words. It was very great to know how this concept of Robo Twin can make a real difference in the lives of people who are physically separated from their loved ones, for example, *"I feel that this concept is innovative, and it is almost accurate in simulating a handshake with a real person. This is something that people can consider using when they'd want to feel closer with their loved ones", "Really cool I love the idea of the hand and using it for long distance. Reminds me of the love bracelet for long distance friends and couples to show you are thinking of them with a tap on the screen".*

However, some participants commented on the size of the Robo Twin hand, particularly female participants, where they mentioned how hard it was for them to completely grasp the Robo Twin hand while performing the handshake, for example, *"I feel that I wasn't able to get the best use out of the sensors of the hand because my hands were too small to reach all of them", Very intuitive and fairly natural, however the hand was a bit large to grasp naturally while also*

hitting the sensors". This definitively opened an area of improvement for the Robo Twin hand design which will be taken into consideration in its future improvement aspects.

5.4.2 Quantitative Analysis

In this section, we analyzed the handshake data resulting from the handshake experiment performed by participants with our Robo Twin arm. Our Robo Twin arm design helped us to collect the data and to study the various characteristics of the human handshake such as the average duration of handshake, average and maximum force applied by the participants over the period of their handshake, average temperature of the participant's palm and fingertips as sensed by our Robo Twin. These finding were then used to comment on the handshake characteristics differences across gender and towards the personality traits of the participants.

1. Duration of handshake (in seconds): The time taken for each participant to complete a handshake with our Robo Twin hand is calculated as the difference in timestamps associated with the start and end of the recorded sensor data, which is nothing but the beginning and end of the handshake experiment. The time taken by each participant to initiate and end the handshake with our Robo Twin hand is summarized in the Figure 5.3.

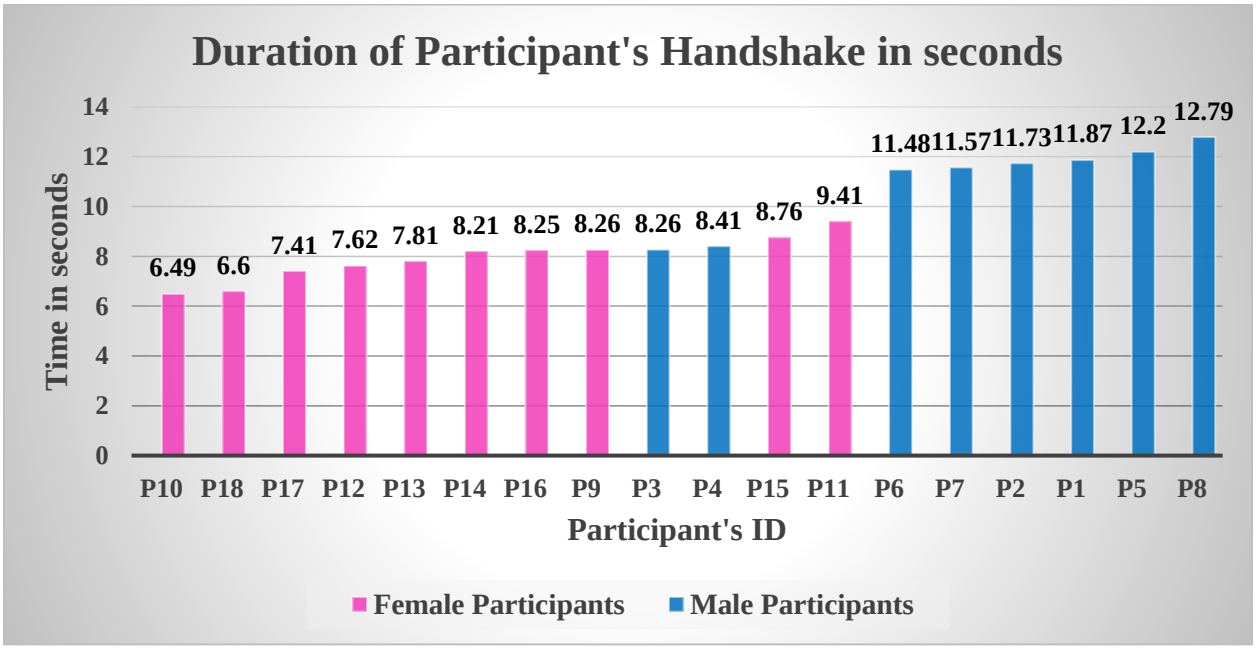

Figure 5.3 Time taken by each participant to complete a handshake with Robo Twin

The Figure 5.3 represents the average time taken by both male and female participants to complete a handshake. On average the duration of handshake for females is ‘7.88 secs’ whereas for male participants it’s ‘11.03 secs’, approximately ‘3 secs’ longer than the female participants.

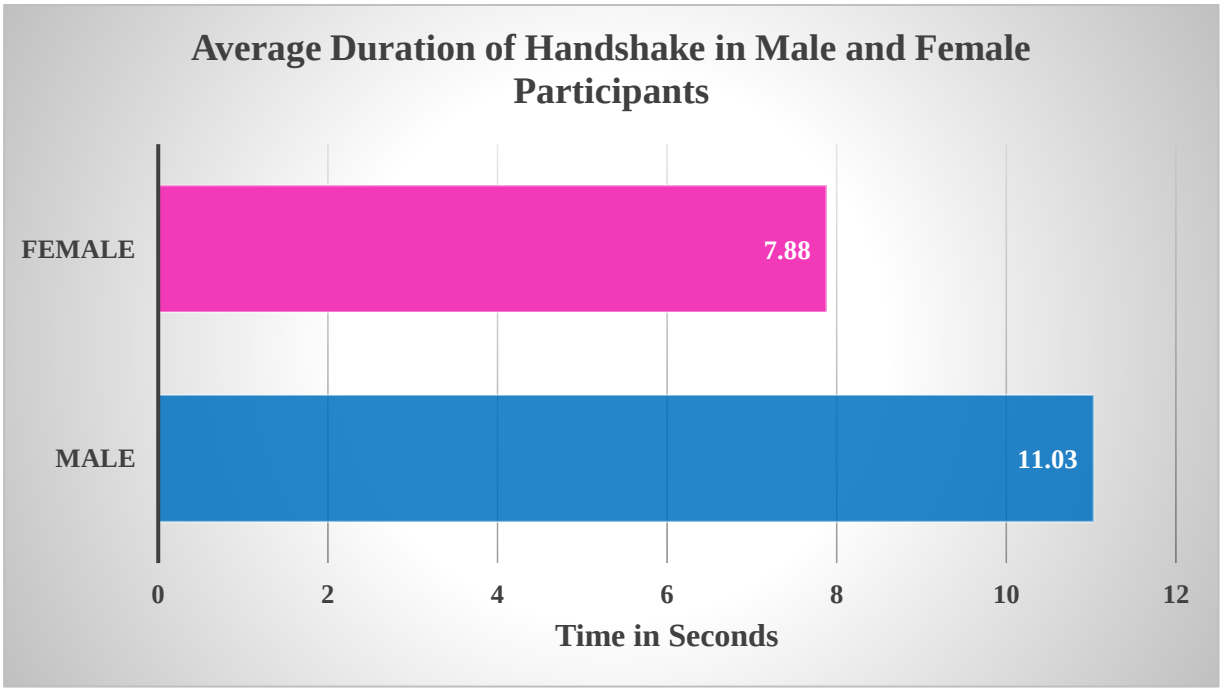

Figure 5.4 Average time taken by male and female participants to complete a handshake

The results obtained are in accordance with the research study in [12] which states that across gender, male tends to have longer duration of handshakes than their female counterparts. This average duration of handshake across both male and female gender is illustrated in the Figure 5.4.

2. Average force applied (in Newtons): The average force applied by each participant while performing a handshake is the average value sensed by all pressure sensors placed on the Robo Twin hand over the period of each participant’s handshake. Figure 5.5 represents the overall average force applied by each individual participant while making a handshake with the Robo Twin hand.

We can observe that most of the male participants have the highest values of average force applied while performing a handshake than the female participants. By averaging these values of applied force by both individual male and female participants, it is found that males tend to apply comparatively more force than their female counterparts, in conformity with [12], [14].

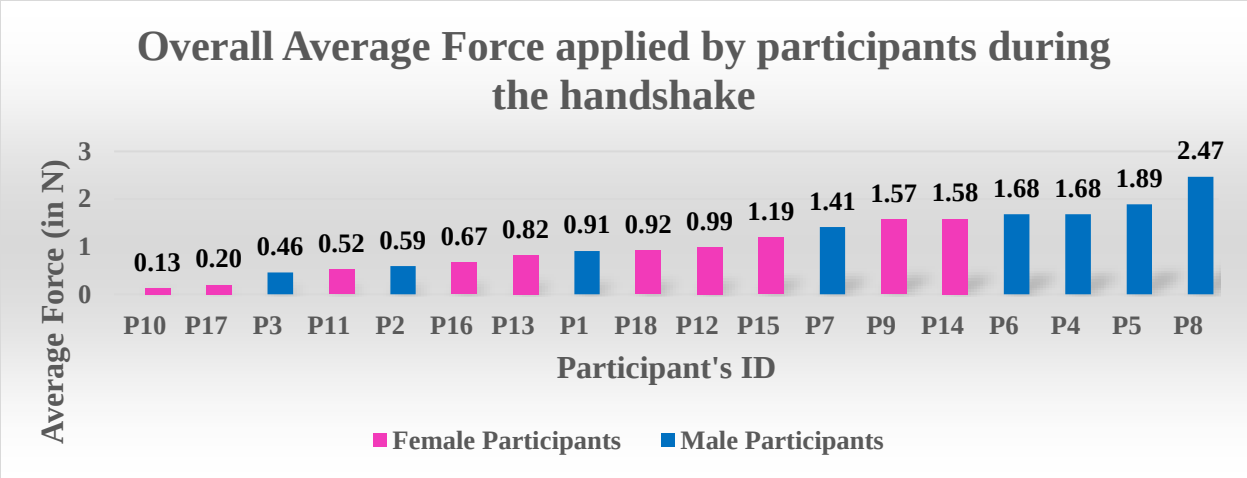

Figure 5.5 Overall average force applied by each participant during their period of handshake

However, research study in [13] which measures the hand grip strength in young men, women and highly trained female athletes, using a handheld hand grip ergometer instead of a human providing ratings as in [12], states that 5% of female participants applied more pressure/force than 10% of male participants. Therefore, not all males will have higher values of applied pressure/force than the females and not all females will have lesser values of applied pressure/force than males.

3. Maximum force applied (in Newtons): The maximum applied force is the maximum value of force sensed by the FSR sensors placed on the hand, during the entire course of handshake, by the participant. It is found that the maximum force that a male candidate applied during his course of handshake with the Robo Twin arm is *10.08 N* while a female candidate applied a maximum of *5.97 N*. Figure 5.6 provide details on maximum force applied by each individual participant during their entire course of handshake.

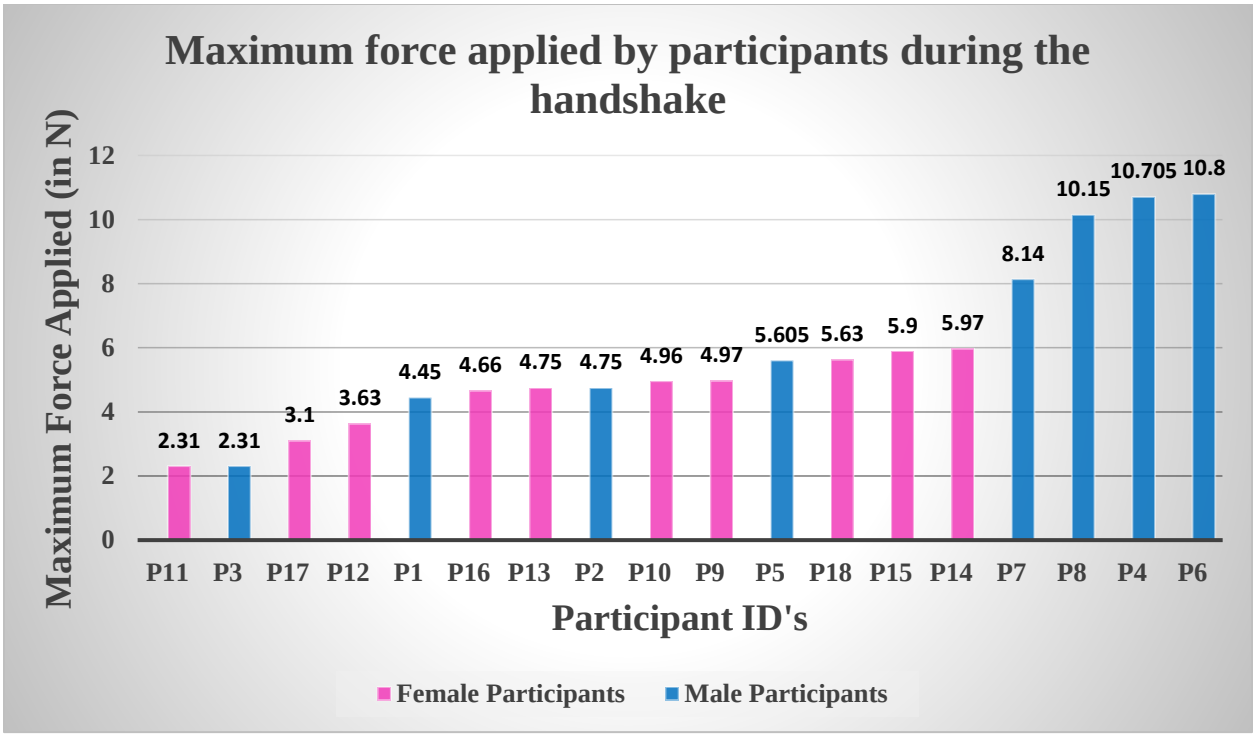

Figure 5.6 Maximum force applied by each participant during the handshake

Calculating the average of maximum applied force across gender, we see that this average in females is at 4.58 N whereas in males it's at 7.11 N. Hence, whether it is average force or maximum force applied during the handshake, most of the male participants tend to apply significantly more than most of the female participants, as found in [13].

4. Palm & Fingertips Temperature (in °C): With the help of temperature sensors integrated on the palm and hand of the Robo Twin hand, we were able to sense and record the average temperature of the participants palm and fingertips in contact, while performing a handshake. A total of four temperature sensors were placed on the Robo Twin's palm to estimate the average of the participants palm temperature and one temperature sensor is placed at the backside of the Robo Twin hand to sense the temperature of the thumb fingertip of the participant's hand which implies the temperature of all fingertips as they are all maintained at almost the same temperature value at any given instant of time. The average of four temperature sensors placed on the palm for all participants is represented in the Figure 5.7.

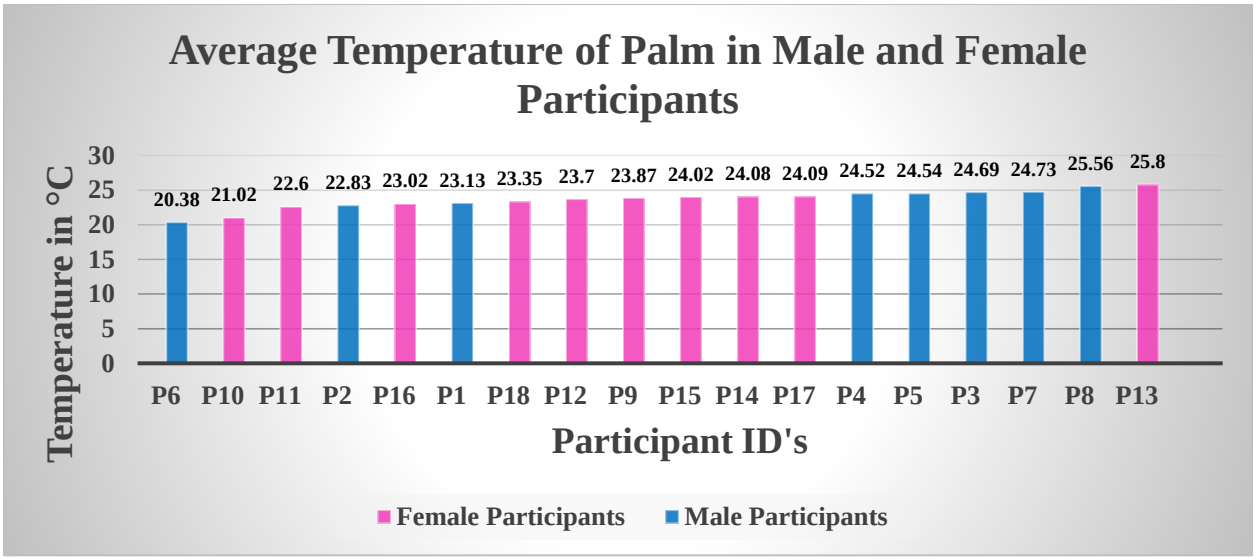

Figure 5.7 Participants average temperature of the palm in °C

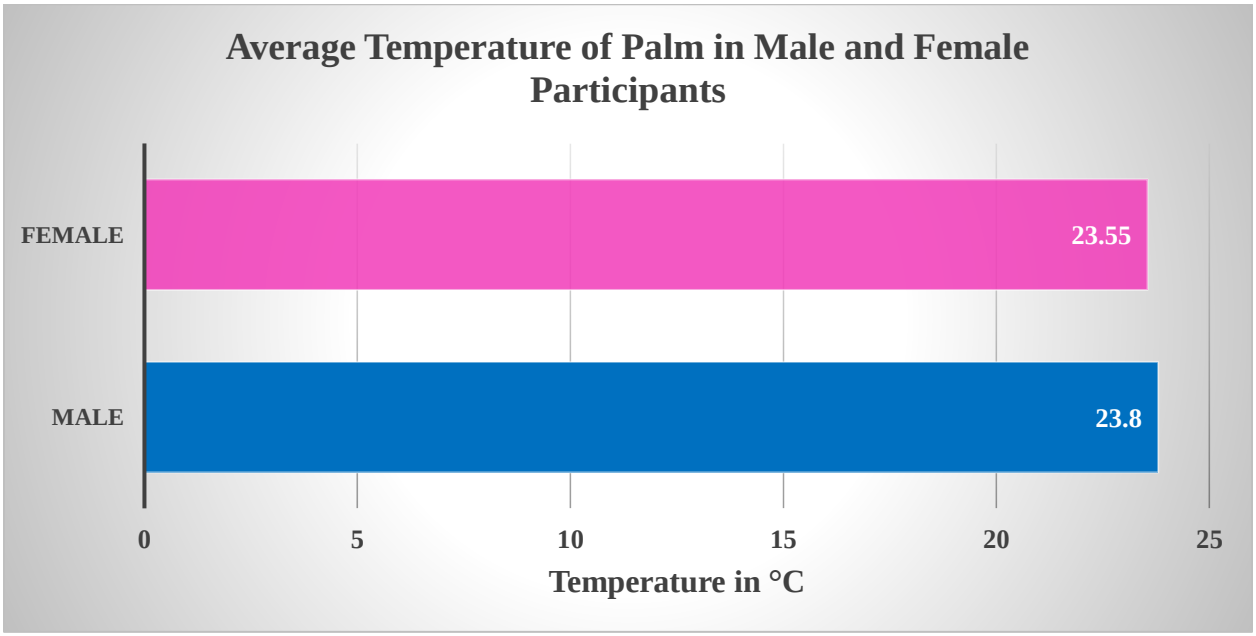

Figure 5.8 Average temperature of palm in male and female participants in °C

Although the average temperature is nearly the same for all participants, male candidates tend to have slightly more average temperature than the female candidates. The overall, average palm's temperature for female participants is 23.55°C and for male participants it 23.8°C, illustrated in the Figure 5.8.

Similarly, male participants demonstrated a higher average fingertips temperature than their female counterparts. Figure 5.9 represents the average fingertips temperature for all individual participants.

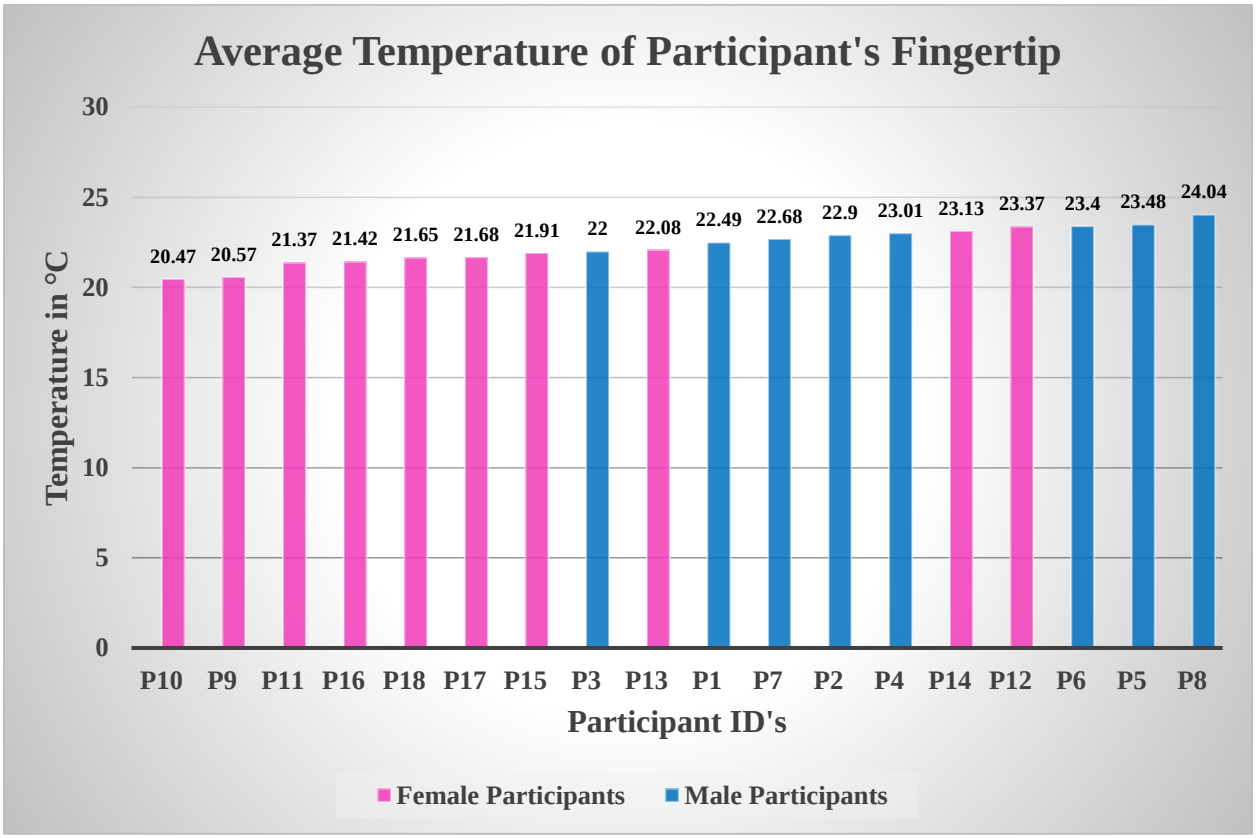

Figure 5.9 Average temperature of participant's fingertips in °C

Overall, male participants on an average maintained their fingertips temperature at 23°C whereas the female participants maintained their average fingertips temperature at 21.76°C, a 1.24°C higher than the males average fingertip temperature, this is illustrated in Figure 5.10.

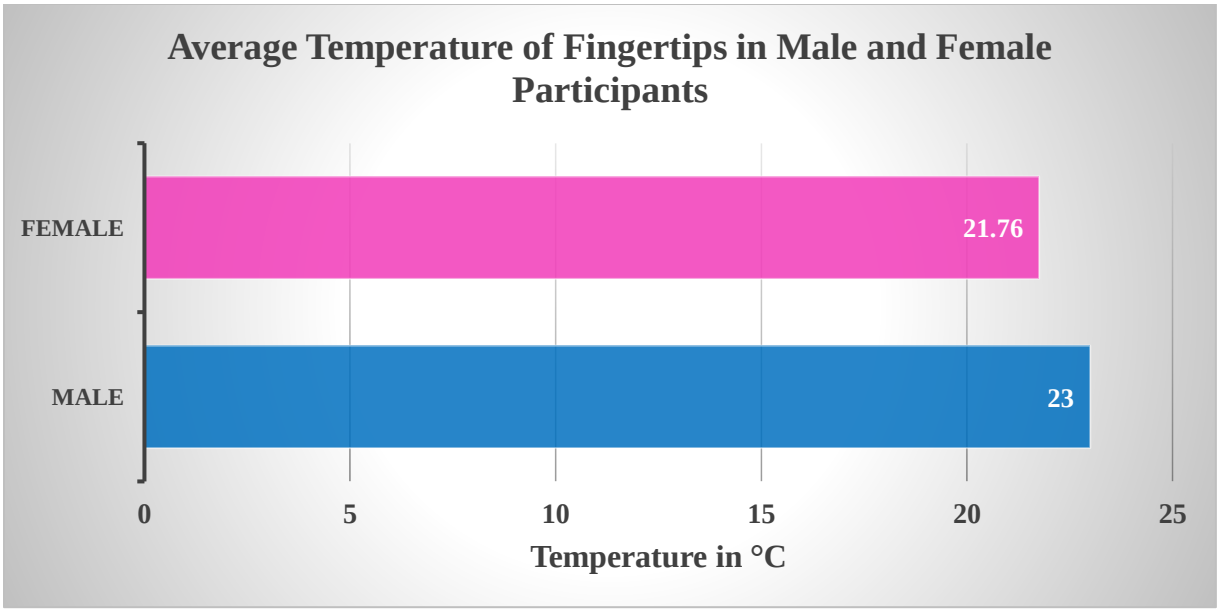

Figure 5.10 Average fingertips temperature in male and female participants

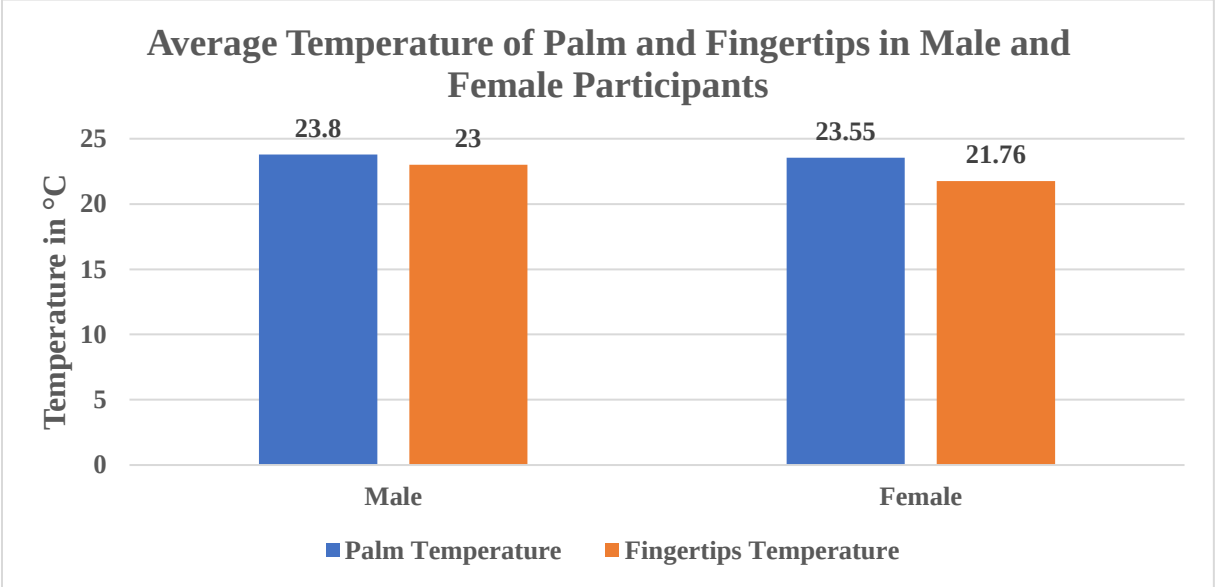

Figure 5.11 Average palm and fingertips temperature in male and female participants

Therefore, whether its average temperature of the palm or the fingertips, the male participants maintained at a bit higher value than the female participants. Across the palm and fingertips temperature, whether its male or female participants, we noticed that the palm of the participants hand is maintained at a higher temperature than the fingertips. This is demonstrated in the Figure 5.11.

5. Personality and Handshaking characteristics: The participant's personality traits were assessed through a report generated by ITP Metric platform, based on the responses to the questionnaires that the participants completed. This report outlines the level of each participant's five personality factors such as extraversion, emotional, conscientiousness, agreeableness, and openness. The score for each trait is presented in percentile form with grey lines separating each decile. The yellow vertical lines represent the breakpoints between ***'Low'*** (between 0^{th} and 25^{th} percentile), ***'Moderate'*** (between 25^{th} and 75^{th} percentile) and finally ***'High'*** (more than 75^{th} percentile).

Across the male gender, we found that the participants who applied least pressure and had low duration while making a handshake were high on conscientiousness and emotionality, but low on extroversion, agreeableness, and open to experience scales. While participant's who applied the most pressure and had longer duration were high on conscientious, agreeableness and open to experience, but were low to moderate on extraversion and emotionality scales. We represent these results by a four-quadrant plot with 'Duration' on X-axis and 'Average applied pressure' on Y-axis in Figure 5.12 below.

Across the female gender, we found that the participants with firmer handshakes are more open to experience only if they are high on conscientious, emotionality, agreeableness and low to moderate on extraversion scales of personality traits. While the participants with less firmer handshakes were found to be less to open to experience provided, they are low on conscientiousness and agreeableness, moderate on emotionality and low to moderate on extraversion scales of personality traits.

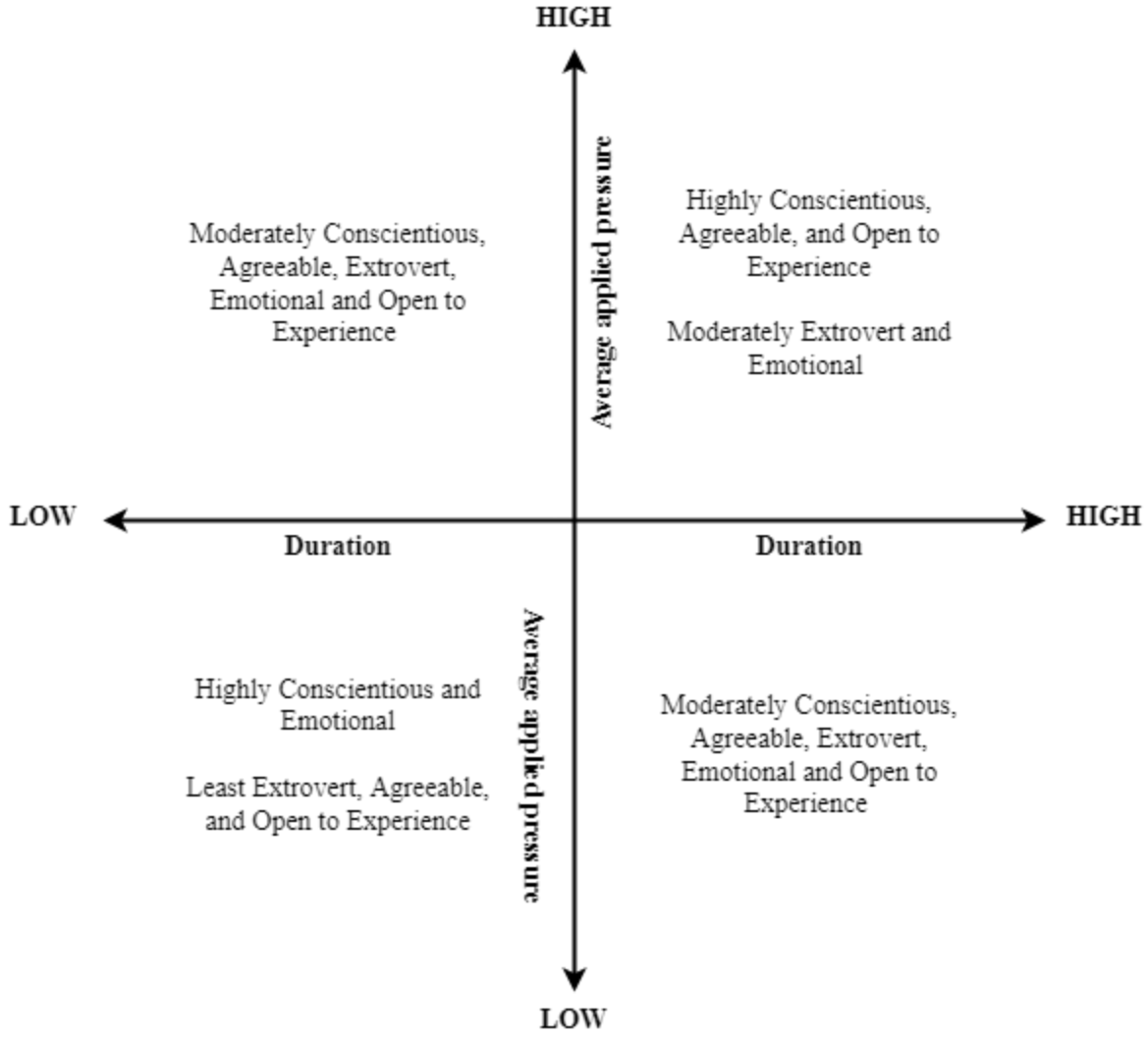

Figure 5.12 Four quadrant plot of personality traits in male participants across duration and average applied pressure.

The results obtained are in conformity with [12], [54] that the individuals with longer ad firmer handshakes are more open to experience. However, we believe that to be able to comment more on the correlation between personality traits and handshaking characteristics a larger data set is needed.

5.5 Summary

In this chapter, we evaluated our Robo Twin system for making a handshake with physically distant person, both qualitatively and quantitatively. Through a post experiment questionnaire, a higher percentage of participants demonstrated that they are likely to use and adopt Robo Twin system for performing a handshake with their loved ones separated by a physical distance.

Our design of Robo Twin arm helped us analyse the different characteristics of human handshake across gender and their correlation to their personality traits. The handshaking characteristics includes the duration of handshake, average and maximum force applied, and average temperature of palm and fingertips of the participating individuals. Whether its average or maximum force applied during the handshake or temperature of both palm and fingertips, male participants have an upper hand compared to the female participants. Also, individuals with longer and firmer handshakes were found to be more open to experience that their counterparts.

6. Conclusions and Future Work

6.1 Conclusion

In this thesis, we reviewed the existing literature in the field of Digital Twin robotic representation with a focus on Digital Twin robotic arm and found that a very limited number of research works were proposed in this domain and much more work still needs to be achieved. Overall, we found that the DT robotic arm needs to incorporate multi-modal haptic sensing. It should provide a good accuracy in terms of temperature sensing and pressure sensing, while keeping the cost low enough for use by the public. Additionally, it should provide human-like characteristics, which can be challenging, such as the emulation of human skin to provide a realistic handshake.

Based on our findings from the related work, we proposed the concept of Robo Twin and put forward the design and implemented the physical representation of the Digital Twin's robotic arm capable of closely imitating the human handshake. To keep the overall cost low, we selected a highly under-actuated anthropomorphic robotic arm design by Inmoov, which makes use of the existing additive manufacturing technology. This design is then integrated with temperature and pressure sensors and vibrotactile pressure actuators to achieve the task of sensing pressure, temperature and actuating the received force feedback.

This thesis also attempts to bridge the gap in the existing research in analyzing the sensors and actuators placement on the robotic hand to accurately provide the natural handshake experience with our Robo Twin hand. A bidirectional serial communication using the available hardware serial ports of the Arduino Mega2560 microcontroller on either side of the Robo Twin arms is implemented for the transfer of pressure data to actuate the vibration motors to provide gradual and effective force feedback while making a handshake.

Finally, we conducted an experiment to evaluate both the quantitative and qualitative experience with our Robo Twin system by the participants and to understand the potential future developments in the design and concept of our Robo Twin.

6.2 Future Directives

This thesis gives an insight into how difficult it is to provide a set of human skills to a humanoid robot to carry out the complex task of making a handshake. There is a lot of potential research work that can be done to propose ideas and solutions for robotic hands with haptic modalities. From our work outlined in this thesis, and after analyzing the system's performance both qualitatively and quantitatively, we propose the following improvements that needs to be done to make the Robo Twin arm and system in general, more intuitive.

1. From the perspective of Robo Twin's arm design, it needs to be modified to accommodate both male and female hand sizes, as few of our female participants highlighted that they felt that the size of the Robo Twin arm was bulky for them to completely grasp its hand as they would normally do while performing a handshake with any other person.

2. Since our main concept of Robo Twin system is to allow people perform a handshake remotely, there is a need of having a communication network that would allow the transmission and reception of such sensory data to achieve a virtual handshake remotely on the other side of the system.

3. As mentioned, both temperature and pressure are most important sensory and motor functions of the human hand, therefore the advanced version of Robo Twin arm will have to incorporate temperature actuators to actuate the sensed temperature on the other arm like the pressure, to improve the user's experience and feeling of a handshake with the Robo Twin system.

Hence, further research is warranted to answer part of these questions and provide more insights towards the design and development of the DT robotic representation.

References

[1] J. Huang, P. Sun, and W. Zhang, “Analysis of the Future Prospects for the Metaverse,” *Adv. Econ. Bus. Manag. Res.*, vol. 648, no. Icfied, pp. 1899–1904, 2022.

[2] Mm. MFNAmirulloh, “Know More Metaverse as The Technology of The Future,” *Int. J. Res. Appl. Technol.*, vol. 2, no. 2, pp. 174–177, 2022.

[3] D. Gelernter, *Mirror Worlds*. Oxford University Press, 1991.

[4] M. Grieves and J. Vickers, “Digital Twin: Mitigating UnpredicTable, Undesirable Emergent Behavior in Complex Systems,” in *Transdisciplinary Perspectives on Complex Systems*, Cham: Springer International Publishing, 2017, pp. 85–113.

[5] K. M. Alam and A. El Saddik, “C2PS: A Digital Twin Architecture Reference Model for the Cloud-Based Cyber-Physical Systems,” *IEEE Access*, vol. 5, pp. 2050–2062, 2017, doi: 10.1109/ACCESS.2017.2657006.

[6] A. El Saddik, “Digital Twins: The Convergence of Multimedia Technologies,” *IEEE Multimed.*, vol. 25, no. 2, pp. 87–92, 2018, doi: 10.1109/MMUL.2018.023121167.

[7] A. El Saddik, F. Laamarti, and M. Alja’Afreh, “The Potential of Digital Twins,” *IEEE Instrum. Meas. Mag.*, vol. 24, no. 3, pp. 36–41, 2021, doi: 10.1109/mim.2021.9436090.

[8] F. Arafsha, F. Laamarti, and A. El Saddik, “Cyber-physical system framework for measurement and analysis of physical activities,” *Electron.*, vol. 8, no. 2, 2019, doi: 10.3390/electronics8020248.

[9] A. El Saddik *et al.*, “Dtwins: A Digital Twins Ecosystem for Health and Well-Being,” *IEEE COMSOC MMTC Commun. - Front.*, vol. 14, no. 2, pp. 39–43, 2019.

[10] F. Laamarti, H. F. Badawi, Y. Ding, F. Arafsha, B. Hafidh, and A. El Saddik, “An ISO/IEEE 11073 Standardized Digital Twin Framework for Health and Well-Being in Smart Cities,” *IEEE Access*, vol. 8, pp. 105950–105961, 2020, doi: 10.1109/ACCESS.2020.2999871.

[11] R. Ferdousi, F. Laamarti, M. A. Hossain, C. Yang, and A. El Saddik, “Digital twins for well-being: an overview,” *Digit. Twin*, vol. 1, p. 7, 2022, doi: 10.12688/digitaltwin.17475.2.

[12] W. F. Chaplin, J. B. Phillips, J. D. Brown, N. R. Clanton, and J. L. Stein, “Handshaking, gender, personality, and first impressions.,” *J. Pers. Soc. Psychol.*, vol. 79, no. 1, pp. 110–117, 2000, doi: 10.1037/0022-3514.79.1.110.

[13] D. Leyk *et al.*, “Hand-grip strength of young men, women and highly trained female athletes,” *Eur. J. Appl. Physiol.*, vol. 99, no. 4, pp. 415–421, 2007, doi: 10.1007/s00421-006-0351-1.

[14] P. H. Orefice, M. Ammi, M. Hafez, and A. Tapus, “Let’s handshake and I’ll know who you are: Gender and personality discrimination in human-human and human-robot handshaking interaction,” *IEEE-RAS Int. Conf. Humanoid Robot.*, pp. 958–965, 2016, doi: 10.1109/HUMANOIDS.2016.7803388.

[15] D. N. Nenchev, A. Konno, and T. Tsujita, “Introduction,” *Humanoid Robot.*, pp. 1–14, 2019, doi: 10.1016/b978-0-12-804560-2.00008-0.

[16] “Honda debuts new humanoid robot ‘ASIMO,’” *Ind. Robot An Int. J.*, vol. 28, no. 2, Apr. 2001, doi: 10.1108/ir.2001.04928bab.002.

[17] “ASIMO by Honda | The World’s Most Advanced Humanoid Robot.” https://asimo.honda.com/asimo-specs/ (accessed Dec. 14, 2021).

[18] K. Kaneko *et al.*, “Design of prototype humanoid robotics platform for HRP,” in *IEEE/RSJ International Conference on Intelligent Robots and System*, 2002, vol. 3, pp. 2431–2436, doi: 10.1109/IRDS.2002.1041632.

[19] “Topio – Robotic Infrastructure & Services Provider | Robot Center.” https://www.robotcenter.co.uk/products/humanoid-robot-hrp-4?variant=187380732 (accessed Dec. 14, 2021).

[20] K. Kaneko *et al.*, “Humanoid robot HRP-2,” in *IEEE International Conference on Robotics and Automation, 2004. Proceedings. ICRA ’04. 2004*, 2004, no. April, pp. 1083-1090 Vol.2, doi: 10.1109/ROBOT.2004.1307969.

[21] K. Kaneko, K. Harada, F. Kanehiro, G. Miyamori, and K. Akachi, “Humanoid robot HRP-3,” in *2008 IEEE/RSJ International Conference on Intelligent Robots and Systems*, Sep. 2008, pp. 2471–2478, doi: 10.1109/IROS.2008.4650604.

[22] “Fujitsu Introduces Miniature Humanoid Robot, HOAP-1.” https://pr.fujitsu.com/en/news/2001/09/10.html (accessed Dec. 14, 2021).

[23] D. Gouaillier *et al.*, “Mechatronic design of NAO humanoid,” *Proc. - IEEE Int. Conf. Robot. Autom.*, pp. 769–774, 2009, doi: 10.1109/ROBOT.2009.5152516.

[24] “Pepper and NAO in the service of the Healthcare sector | SoftBank Robotics EMEA.” https://www.softbankrobotics.com/emea/en/pepper-and-nao-robots-education (accessed Jul. 04, 2021).

[25] L. Wu, M. Larkin, A. Potnuru, and Y. Tadesse, “HBS-1: A modular child-size 3D printed humanoid,” *Robotics*, vol. 5, no. 1, 2016, doi: 10.3390/robotics5010001.

[26] G. Langevin, “InMoov open-source 3D printed life-size robot,” *pp. URL: http://inmoov. fr, License: http://creativecommons. org/licenses/by–nc/3.0/legalcode*. 2014.

[27] R. Siemasz, K. Tomczuk, and Z. Malecha, “3D printed robotic arm with elements of artificial intelligence,” *Procedia Comput. Sci.*, vol. 176, pp. 3741–3750, 2020, doi: 10.1016/j.procs.2020.09.013.

[28] M. Arns, T. Laliberte, and C. Gosselin, “Design, control and experimental validation of a haptic robotic hand performing human-robot handshake with human-like agility,” *IEEE Int. Conf. Intell. Robot. Syst.*, vol. 2017-Septe, pp. 4626–4633, 2017, doi: 10.1109/IROS.2017.8206333.

[29] L. Tian, N. M. Thalmann, J. Zheng, and D. Thalmann, “Design of a Highly Biomimetic and Fully-Actuated Robotic Finger,” in *2019 IEEE Symposium Series on Computational Intelligence (SSCI)*, Dec. 2019, pp. 2382–2387, doi: 10.1109/SSCI44817.2019.9002870.

[30] O. Shorthose, A. Albini, L. He, and P. Maiolino, “Design of a 3D-Printed Soft Robotic Hand With Integrated Distributed Tactile Sensing,” *IEEE Robot. Autom. Lett.*, vol. 7, no. 2, pp. 3945–3952, 2022, doi: 10.1109/LRA.2022.3149037.

[31] T. Feix, J. Romero, H. B. Schmiedmayer, A. M. Dollar, and D. Kragic, “The GRASP Taxonomy of Human Grasp Types,” *IEEE Trans. Human-Machine Syst.*, vol. 46, no. 1, pp. 66–77, 2016, doi:

10.1109/THMS.2015.2470657.

[32] S. Shin, S. Han, K. Lee, Hyungpil Moon, H. R. Choi, and J. C. Koo, “A design framework for dexterous robotic hand,” *URAI 2011 - 2011 8th Int. Conf. Ubiquitous Robot. Ambient Intell.*, pp. 539–541, 2011, doi: 10.1109/URAI.2011.6145878.

[33] M. Ntagios, H. Nassar, A. Pullanchiyodan, W. T. Navaraj, and R. Dahiya, “Robotic Hands with Intrinsic Tactile Sensing via 3D Printed Soft Pressure Sensors,” *Adv. Intell. Syst.*, vol. 2, no. 6, p. 1900080, 2020, doi: 10.1002/aisy.201900080.

[34] Z. Kappassov, Y. Khassanov, A. Saudabayev, A. Shintemirov, and H. A. Varol, “Semi-anthropomorphic 3D printed multigrasp hand for industrial and service robots,” *2013 IEEE Int. Conf. Mechatronics Autom. IEEE ICMA 2013*, no. c, pp. 1697–1702, 2013, doi: 10.1109/ICMA.2013.6618171.

[35] S. Li, R. Rameshwar, A. M. Votta, and C. D. Onal, “Intuitive Control of a Robotic Arm and Hand System with Pneumatic Haptic Feedback,” *IEEE Robot. Autom. Lett.*, vol. 4, no. 4, pp. 4424–4430, 2019, doi: 10.1109/LRA.2019.2937483.

[36] D. Lanigan and Y. Tadesse, “Low Cost Robotic Hand that Senses Heat and Pressure,” 2017.

[37] F. Salman, Y. Cui, Z. Imran, F. Liu, L. Wang, and W. Wu, “A Wireless-controlled 3D printed Robotic Hand Motion System with Flex Force Sensors,” *Sensors Actuators, A Phys.*, vol. 309, p. 112004, 2020, doi: 10.1016/j.sna.2020.112004.

[38] “A Patient’s Guide to Hand Anatomy.” https://eorthopod.com/hand-anatomy/ (accessed Jul. 21, 2022).

[39] J. Beaudoin, T. Laliberte, and C. Gosselin, “Haptic Interface for Handshake Emulation,” *IEEE Robot. Autom. Lett.*, vol. 4, no. 4, pp. 4124–4130, 2019, doi: 10.1109/lra.2019.2931221.

[40] J. Avelino, T. Paulino, C. Cardoso, R. Nunes, P. Moreno, and A. Bernardino, “Towards natural handshakes for social robots: Human-Aware hand grasps using tactile sensors,” *Paladyn*, vol. 9, no. 1, pp. 221–234, 2018, doi: 10.1515/pjbr-2018-0017.

[41] L. Wang, J. DelPreto, S. Bhattacharyya, J. Weisz, and P. K. Allen, “A highly-underactuated robotic hand with force and joint angle sensors,” *IEEE Int. Conf. Intell. Robot. Syst.*, pp. 1380–1385, 2011, doi: 10.1109/IROS.2011.6048748.

[42] Y. Wang, Y. Lu, D. Mei, and L. Zhu, “Liquid Metal-Based Wearable Tactile Sensor for Both Temperature and Contact Force Sensing,” *IEEE Sens. J.*, vol. 21, no. 2, pp. 1694–1703, 2021, doi: 10.1109/JSEN.2020.3015949.

[43] T. Bhattacharjee, J. Wade, Y. Chitalia, and C. C. Kemp, “Data-driven thermal recognition of contact with people and objects,” *IEEE Haptics Symp. HAPTICS*, vol. 2016-April, pp. 297–304, 2016, doi: 10.1109/HAPTICS.2016.7463193.

[44] M. Soni, M. Bhattacharjee, M. Ntagios, and R. Dahiya, “Printed Temperature Sensor Based on PEDOT: PSS-Graphene Oxide Composite,” *IEEE Sens. J.*, vol. 20, no. 14, pp. 7525–7531, 2020, doi: 10.1109/JSEN.2020.2969667.

[45] T. Someya, “Building bionic skin,” *IEEE Spectr.*, vol. 50, no. 9, pp. 50–56, 2013, doi: 10.1109/MSPEC.2013.6587191.

[46] P. Weiner, C. Neef, and T. Asfour, “A Multimodal Embedded Sensor System for Scalable Robotic and Prosthetic Fingers,” in *2018 IEEE-RAS 18th International Conference on Humanoid Robots (Humanoids)*, Nov. 2018, pp. 286–292, doi: 10.1109/HUMANOIDS.2018.8624955.

[47] C. Yu, L. Lindenroth, J. Hu, J. Back, G. Abrahams, and H. Liu, “A vision-based soft somatosensory system for distributed pressure and temperature sensing,” *IEEE Robot. Autom. Lett.*, vol. 5, no. 2, pp. 3323–3329, 2020, doi: 10.1109/LRA.2020.2974649.

[48] B. Mirkovic and D. Popovic, “Prosthetic hand sensor placement: Analysis of touch perception during the grasp,” *Serbian J. Electr. Eng.*, vol. 11, no. 1, pp. 1–10, 2014, doi: 10.2298/sjee131004001m.

[49] A. M. Almassri *et al.*, “Pressure sensor: State of the art, design, and application for robotic hand,” *J. Sensors*, vol. 2015, 2015, doi: 10.1155/2015/846487.

[50] A. Khasnobish, M. Pal, D. Sardar, D. N. Tibarewala, and A. Konar, “Vibrotactile feedback for conveying object shape information as perceived by artificial sensing of robotic arm,” *Cogn. Neurodyn.*, vol. 10, no. 4, pp. 327–338, 2016, doi: 10.1007/s11571-016-9386-0.

[51] R. B. Mishra, S. M. Khan, S. F. Shaikh, A. M. Hussain, and M. M. Hussain, “Low-cost foil/paper based touch mode pressure sensing element as artificial skin module for prosthetic hand,” *2020 3rd IEEE Int. Conf. Soft Robot. RoboSoft 2020*, pp. 194–200, 2020, doi: 10.1109/RoboSoft48309.2020.9116035.

[52] “The BIG FIVE Personality Assessment.” https://www.itpmetrics.com/.

[53] “Positive Affect and Negative Affect Score.” https://psytests.org/emotional/panas.html.

[54] W. F. Chaplin *et al.*, “Let’s handshake and I’ll know who you are: Gender and personality discrimination in human-human and human-robot handshaking interaction,” *J. Pers. Soc. Psychol.*, vol. 79, no. 1, pp. 958–965, 2016, doi: 10.1037/0022-3514.79.1.110.